AD-A125 822 THE INTERACTION OF SHORT-WAVELENGTH INTERNAL WAVES WITH 1/1
A BACKGROUND CURRENT(U) SCRIPPS INSTITUTION OF
OCEANOGRAPHY LA JOLLA CA D BROUTMAN DEC 82
UNCLASSIFIED SIO-REF-82-31 N00014-80-C-0440 F/G 8/3 NL

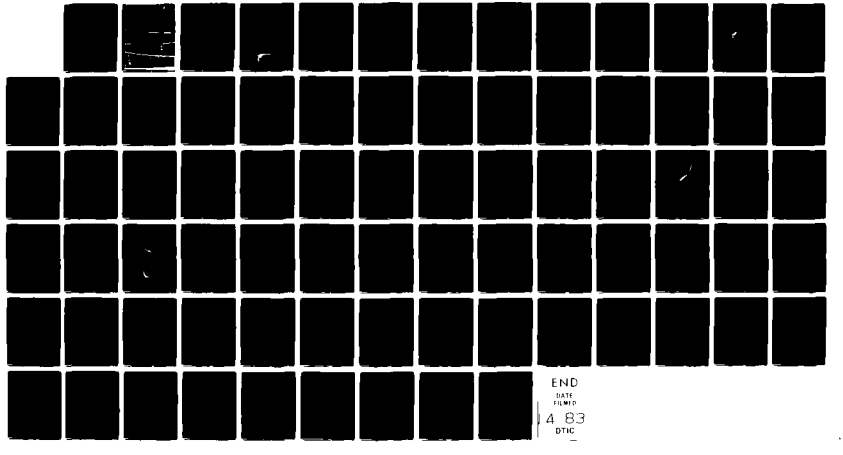

END
DATE FILMED
4 83
DTIC

M-2

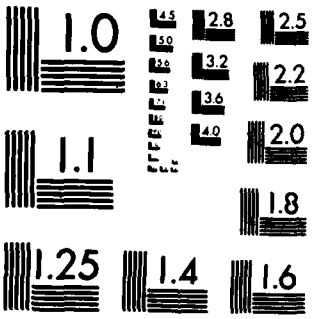

# SIO REFERENCE SERIES

## THE INTERACTION OF SHORT-WAVELENGTH INTERNAL WAVES WITH A BACKGROUND CURRENT

by

Dave Brueshaber







December 1982

SIO Ref. No. 82-31

University of California, San Diego, Institute of Oceanography

Unclassified

SECURITY CLASSIFICATION OF THIS PAGE (When Data Entered)

| REPORT DOCUMENTATION PAGE | | READ INSTRUCTIONS BEFORE COMPLETING FORM |
|---|---|---|
| 1. REPORT NUMBER<br>SIO Ref. #82-31 | 2. GOVT ACCESSION NO.<br>AD-A125 827 | 3. RECIPIENT'S CATALOG NUMBER |
| 4. TITLE (and Subtitle)<br>THE INTERACTION OF SHORT-WAVELENGTH INTERNAL WAVES WITH A BACKGROUND CURRENT | | 5. TYPE OF REPORT & PERIOD COVERED<br>6. PERFORMING ORG. REPORT NUMBER |
| 7. AUTHOR(s)<br>Dave Broutman | | 8. CONTRACT OR GRANT NUMBER(s)<br>N00014-80-C-0440 |
| 9. PERFORMING ORGANIZATION NAME AND ADDRESS<br>Scripps Institution of Oceanography<br>La Jolla, CA 92093 | | 10. PROGRAM ELEMENT, PROJECT, TASK AREA & WORK UNIT NUMBERS |
| 11. CONTROLLING OFFICE NAME AND ADDRESS<br>Office of Naval Research<br>Arlington, VA 22217 | | 12. REPORT DATE<br>December 1982<br>13. NUMBER OF PAGES<br>74 |
| 14. MONITORING AGENCY NAME & ADDRESS(if different from Controlling Office) | | 15. SECURITY CLASS. (of this report)<br>Unclassified<br>15a. DECLASSIFICATION/DOWNGRADING SCHEDULE |

16. DISTRIBUTION STATEMENT (of this Report)

Approved for public release. Distribution unlimited.

17. DISTRIBUTION STATEMENT (of the abstract entered in Block 20, if different from Report)

18. SUPPLEMENTARY NOTES

19. KEY WORDS (Continue on reverse side if necessary and identify by block number)

20. ABSTRACT (Continue on reverse side if necessary and identify by block number)

Two approaches are used to explore the effects of shear on short-wavelength internal waves. In the first, the Taylor-Goldstein equation is solved exactly. The solutions show that the amplitude of partially reflected waves is exponentially small as $\underline{c}+\underline{U}_0$, where $\underline{c}$ is the horizontal phase speed of the short waves and $\underline{U}_0$ is the maximum mean flow velocity. The solutions also reveal the inaccuracy of WKB predictions where applied to a curved velocity profile with a minimum Richardson number of order unity...

DD FORM 1 JAN 73 1473 EDITION OF 1 NOV 65 IS OBSOLETE

S/N 0102-LF-014-6601

SECURITY CLASSIFICATION OF THIS PAGE (When Data Entered)

UNIVERSITY OF CALIFORNIA, SAN DIEGO

SCRIPPS INSTITUTION OF OCEANOGRAPHY

# The Interaction of Short-wavelength Internal Waves with a Background Current

by

Dave Broutman

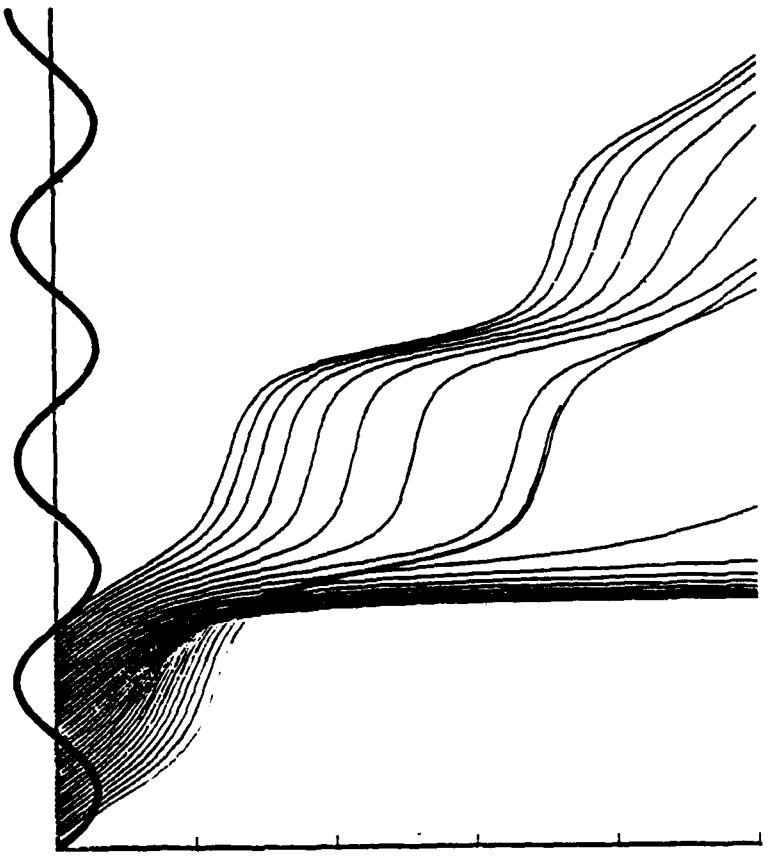

December 1982

SIO Reference No. 82-31

Table of Contents

## List of Figures



## Table Caption

## Acknowledgments

I thank all the members of my thesis committee, particularly my thesis advisor Chip Cox. Discussions with Rob Pinkel, Greg Holloway, and Roger Grimshaw also influenced my direction and accelerated my progress, as did correspondences with Michael McIntyre.

My understanding of ray theory improved through conversations with Joe Keller and George Backus. I appreciate their assistance with the material presented in Chapter 5, Section C and in Appendix B.

I also extend thanks to Mike Freilich, Jose Ochoa, Libe Washburn, John Schedvin, Jeff Lerner, and Carl Gibson.

Deni Menegus typed the thesis, and her expertise in editing saved me time and embarrassment. Prof. John Miles corrected technical and grammatical errors. Chip Cox, Walter Munk, and Russ Davis pointed out weaknesses in an early draft. Don Betts assisted in the planning and preparation of the illustrations.

Finally, I thank the support of Nancy Samuelsen and of Larry Barnett, Jean Loo, Chris Nolting, Angie Nolting, Ken Lisi, Peggy Lasko, Paul Hassig, Wendy Raymond, Mark Wooster, Margaret Ring, Ward Saunders, Bob Darling, Mark Rea, Jim Sinks, Dan Phillips, Tom Deaton, Dana Freidman, Rick Fulcher, and of course, my parents.

This work was funded by the Office of Naval Research.

## VITA

May 18, 1953 — Born — Rochester, New York

| | |
|---|---|
| 1975 | B.A., University of California, Los Angeles |
| 1976-82 | Research Assistant, Teaching Assistant,<br>Scripps Institution of Oceanography,<br>University of California, San Diego |
| 1979-81 | Summer School Instruction,<br>University of California, San Diego |
| 1982 | Summer Fellow in Geophysical Fluid Dynamics,<br>Woods Hole Oceanographic Institution<br>Woods Hole, Massachusetts |
| 1982 | Doctor of Philosophy,<br>Scripps Institution of Oceanography,<br>University of California, San Diego |

## FIELDS OF STUDY

Major Field: Oceanography

Studies in Wave Dynamics
Professors Myrl C. Hendershott, Russ E. Davis, Robert T. Guza, John W. Miles, Walter H. Munk, and Charles S. Cox

Studies in Physical Oceanography
Professors Joseph L. Reid, Myrl C. Hendershott, Walter H. Munk, Charles S. Cox, and Richard L. Salmon

Studies in Fluid Mechanics
Professors Clinton D. Winant and Carl H. Gibson

Studies in Applied Mathematics
Professors Sinai Rand, Donald R. Smith, and John W. Miles

## ABSTRACT OF THE DISSERTATION

The *Interaction of Short-wavelength Internal Waves*

with a Background Current

by

Dave Broutman

Doctor of Philosophy in Oceanography

University of California, San Diego

Scripps Institution of Oceanography, 1982

Professor Charles S. Cox, Chairman

Two approaches are used to explore the effects of shear on short-wavelength internal waves. In the first, the Taylor-Goldstein equation is solved exactly. The solutions show that the amplitude of partially reflected waves is exponentially small as $c \downarrow U_0$, where $c$ is the horizontal phase speed of the short waves and $U_0$ is the maximum mean flow velocity. The solutions also reveal the inaccuracy of WKB predictions when applied to a curved velocity profile with a minimum Richardson number of order unity.

To investigate internal waves in an inertial current, ray calculations are made. This second approach reveals that the process of refractive convergence, which includes the critical-layer interaction as a special case, operates at virtually all phases of the inertial oscillation and

affects short waves of nearly all frequencies. It is also found, in contrast to the results of steady shear analyses, that short waves with phase speeds less that the mean flow maximum can propagate for several inertial periods without becoming unstable, and conversely that waves with initial phase speeds of two or three times the mean flow maximum can quickly become focussed to unstably high amplitudes.

The final section examines the mean flow induced by three-dimensional, low-frequency, internal wave packets. Rotation alters the character of the flow so that the mean momentum is not equal to $E/c$, where $E$ is the intrinsic energy density. The generation of inertial waves by the internal wave field, as found by Hasselmann (1970) for a wave field that is statistically homogeneous in the horizontal, is not predicted by a calculation that incorporates horizontal variations.

# CHAPTER 1

## INTRODUCTION

A challenging feature of the internal wave field is its maintenance of high and uniform energy levels. A central difficulty arises from our poor understanding of the mechanisms by which internal waves dissipate. To understand such mechanisms is to understand that portion of the spectrum where dissipation is most effective: the short wavelengths.

Several factors complicate the analysis of short waves. Because of their small phase velocities, short waves are strongly refracted by background shears. In the deep ocean, these shears are produced predominantly by inertial oscillations and therefore vary in time as well as in space. Short waves are also sensitive to finestructure in the mean density and velocity profiles (Mysak, 1976), and studies of weakly nonlinear waves predict such rapid time scales for the interaction of short waves that according to Holloway (1980) they "contradict their premises".

No single theory can handle all of these processes. In this thesis, we concentrate on one: the effects of shear, particularly inertial shear, on the propagation of short waves. The objective is to explore the mechanisms by which inertial currents refract short waves to unstable amplitudes. The major results are derived from ray-tracing calculations (Chapter 5), with Chapters 3 and 4 devoted to assessing the accuracy of ray theory over the range of conditions typically found in the deep ocean.

One dissipation mechanism to be examined is the critical-layer interaction. A critical layer is defined as the depth at which the horizontal, Doppler-shifted phase velocity equals the mean flow velocity. Within the WKB approximation, the critical-layer interaction appears as a pattern of converging rays (figure 1.1). There is good reason to suspect this critical-layer convergence as important for short-wave dynamics and dissipation. Many studies suggest that a narrow critical-layer region that remains clearly defined is connected with overturning and mean-flow accelerations (Booker & Bretherton, 1967 (hereafter BB); Thorpe, 1981; Koop, 1981; Fritts, 1978), and since short-wave phase speeds typically fall within the range of the currents through which they propagate (Sanford, 1975; Pinkel, 1981), critical-layer conditions are frequently satisfied.

However, for inertial shears, we show in Chapter 5 that convergence develops for short waves with phase speeds two or three times the mean-flow maximum and that convergence is equally likely when critical-layer conditions are not satisfied.

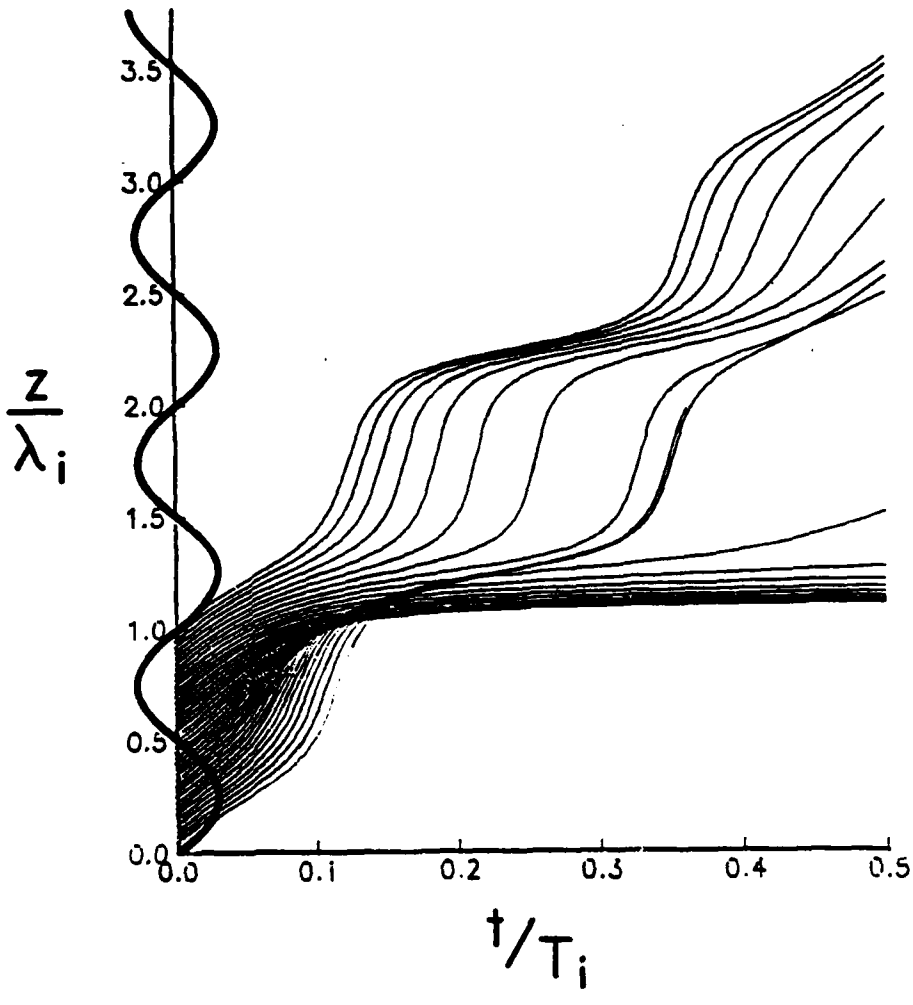


Figure 1.1. Ray trajectories for short waves in an inertial current. The $x$–component of the inertial velocity is given by $U=U_0\sin\beta z\sin ft$, where $\beta=2\pi/\lambda_i$ and $f=2\pi/T_i$ are the inertial wavenumber and frequency respectively. The velocity $U$ is identically zero at $t=0$ and $t=.5T_i$ and attains the profile shown on the vertical axis at $t=.25T_i$. Behavior resembling the critical-layer simulations of Thorpe (1981) begins near $t=.1T_i$ and $z=1.0\lambda_i$, where rays merge.

Rays terminate when the intrinsic energy density $E$ (Chapter 5) surpasses 50 times its initial value or when the Richardson number drops below one-quarter, conditions which arise in more than half of the trajectories. Initial conditions include (see Chapter 5 for notation and assumptions) $k/\beta=.4$, $\omega'/N=.2$, $c/U_0=1.0$, and $J=N^2/(\beta^2U_0^2)=4.0$.

These results are unlike those obtained from the Taylor-Goldstein equation used by BB and in many other critical-layer studies. The Taylor-Goldstein model (or its extension to rotating fluids (Jones, 1967)) is inappropriate for the description of short waves in the deep ocean for at least two reasons. First, it is based on the assumption of steady shears, but as figure 1.1 illustrates, the time dependence associated with inertial currents affects the propagation of short waves within one-tenth of an inertial period. Secondly, the Taylor-Goldstein equation predicts a distribution of wave amplitude and intrinsic frequency in the vertical that applies to, for example, waves produced by steady flow over topography. Short waves in the ocean's interior, however, may be aligned differently, depending in part on their generation mechanism and in part on the way they are refracted by time dependent currents. An example is the case considered by Hartman (1975) and extended to time dependent flows by Thorpe (1978, Appendix). Here, the spread of "critical layers" over a continuous range of depths leads to behavior contrasting the BB results.

Before examining the effects of inertial currents on short waves, a review of the BB and Hartman analyses and a general discussion of critical layers in steady flows is presented in Chapter 2. Then, in preparation for Chapter 5, we estimate the validity of the slowly varying approximation necessary for ray theory. This is begun in Chapter 3 by describing the scales of short waves in the deep ocean and by identifying a criterion for WKB accuracy. In Chapter 4 the magnitude of the energy reflected from strong (but steady) shears is assessed as a possible source for the failure of the WKB approximation.

In Chapter 5, ray theory is used to describe the propagation of short waves in inertial shears. The results are contrasted with the steady-shear predictions reviewed in Chapter 2. The effect of dispersion and geometrical spreading on the convergence of short-wave packets is considered in Chapter 5, Section C. Chapter 6 concludes with a summary and discussion of results.

Parts of the derivations in Chapter 4 and Chapter 5, Section C, are left to Appendices A and B. In Appendix C, which contains its own acknowledgements and references, we examine the mean flow and wake produced by a low-frequency wave packet.

Throughout it is assumed that the Vaisala frequency is constant and that the background current is horizontal with vertical shear, as is produced by an inertial oscillation. Time dependence and rotation are neglected until Chapter 5. The terms background flow and mean flow are used interchangeably even though the mean flow may itself be an internal wave. The mean flow also may have a frequency and vertical wavenumber not much less than the short waves it is refracting but will always be distinguishable by its larger horizontal particle velocities and infinite horizontal scale.

The major conclusions are derived from the results presented in Chapter 5. The results exhibit new ways, not predicted by analyses using steady shears, in which short waves are focussed to unstable amplitudes. These new ways, grouped with the critical-layer interaction, are referred to as *refractive convergence*.

# CHAPTER 2

## BACKGROUND

Two mechanisms proposed for the dissipation of short waves involve refraction by steady shears: the critical-layer interaction and the shear instability of Phillips (1966) and Hartman (1975). These mechanisms are examined in this chapter.

The assumptions of inviscid, small amplitude disturbances in a steady, horizontal current yield a simple model of a critical layer that is described by the Taylor-Goldstein equation. Writing $\mathbf{u}' = (u',0,w')$ with $w'(x,z,t) = w(z)e^{i(kx-\omega t)}$ as the perturbation velocity, k as the horizontal wavenumber, $\omega$ as the Doppler-shifted frequency, $N$ as the Vaisala frequency, $U$ as the mean flow velocity, and $c = \omega/k$ as the Doppler-shifted horizontal phase velocity, the Taylor-Goldstein equation becomes

$$w_{zz} + \left\{ \frac{N^2}{(c-U)^2} + \frac{U_{zz}}{(c-U)} - k^2 \right\} w = 0 \,. \tag{2.1}$$

The critical layer appears as a singular point in the equation and, provided $U_z$ is nonzero at the critical-layer depth, $z_c$, a branch point in the general solution. A series solution to (2.1) reveals that

$$w \sim A(z-z_c)^{1/2+i(Ri-1/4)^{1/2}} + B(z-z_c)^{1/2-i(Ri-1/4)^{1/2}} \,, \tag{2.2}$$

as $z \to z_c$, where $Ri = N^2/U_z^2$ is the local Richardson number and $A$ and $B$ are complex constants. In the unstratified case, $N = 0$ and the addition of a small amount of viscosity removes the singularity. With stratification, both density and momentum become unbounded at the critical layer, so both viscous and thermal diffusion must be included to remove the singularity. The result is then a sixth-order differential equation free of singular points for all values of $c$, which must be examined in the limit of vanishing viscosity and diffusion. For those who prefer second-order differential equations to sixth-order ones, two popular alternatives exist, both of which move the singularity off the real axis into the complex c-plane. Rayleigh damping added to the momentum and density equations is one way to accomplish this (LeBlond and Mysak, 1978), but the proper method is to set up an initial value problem using Laplace transforms (Miles, 1961). The resulting equation need not be solved, only examined to locate the new position of the singular points.

Once the branch is chosen, reflection and transmission coefficients can be computed for waves encountering a critical layer. The overreflection of internal waves was first discovered

in this way (Jones, 1968). The problem with this type of analysis is that although the vertical velocity decreases to zero at the critical layer, virtually nothing else does: the horizontal perturbation velocity, the vertical and horizontal displacements, the perturbation pressure and density, the action density, the intrinsic energy density (see (5.11), and the wave induced shear all become infinite, indicating the inconsistency of the steady state linear theory. For this reason, BB resort to an initial value problem.

Despite the inconsistency, much effort has gone into solving the Taylor-Goldstein equation with various mean flow profiles, density profiles, and boundary conditions for application to internal wave propagation and to the stability of disturbances in a stratified fluid when $Ri < \frac{1}{4}$. In stability theory, solutions with unbounded behavior at the critical layer represent neutral disturbances and lie on curves in the k-Ri plane called singular neutral curves. Miles (1963) proves that contiguous to these curves, unstable solutions exist. Since their phase speeds have nonzero imaginary part, the branch point disappears for real values of $U$ and the inviscid solution is bounded through the depth where $U$, and the real part of $c$ match (Goldstein, 1931).

When applying the Taylor-Goldstein equation to internal wave propagation, the premise is that the steady-state results will match those of a nonsingular analysis except for the region near the critical layer. BB establish that this is so in their initial value problem: "The important point is that, long before [the linear theory becomes invalid], the flow above and below the critical layer has settled down to a steady state with a small decaying oscillation superimposed and that the steady state is the same as that observed by ignoring the details of the critical layer, but matching around it ..." The steady solution predicts a reduction in the flux of pseudomomentum $\overline{u'w'}$ across the critical layer by a factor of $\exp[2\pi(Ri-1/4)^{1/2}]$.

The dynamics of critical-layer interactions are best understood within the WKB approximation (Bretherton, 1966). As a group of waves propagates toward a critical layer, refraction causes the intrinsic frequency and group velocity to decrease. The total action of the group remains constant, but because it is crowded into a smaller volume, the action density grows. Though not conserved, the intrinsic energy density $E$ is similarly amplified through convergence induced by the currents.

A second type of dissipation mechanism for short waves, originally proposed in Phillips (1966, first edition only), is more thoroughly explored by Hartman (1975). Hartman studies a wave packet in a current of constant shear under restrictions that limit dispersion and geometrical spreading due to the variations of group velocity of the Fourier components. The intrinsic frequency $\omega'$ (related to the Doppler-shifted frequency $\omega$ by $\omega = \omega' + Uk$ for $k > 0$) and the vertical wavenumber $m$ satisfy

$$\frac{\delta\omega'}{\omega'_c} \ll 1\,, \quad \frac{\delta m}{m_c} \ll 1\,, \tag{2.3a,b}$$

where $\delta\omega'$ and $\delta m$ are the changes over a distance of one inverse wavenumber, and the subscript $c$ denotes the center value for the packet. A fixed observer sees roughly the same intrinsic frequency everywhere but sees a wide range of Doppler-shifted frequencies because $U$ varies over the vertical dimension of the packet. In the steady solutions to the Taylor-Goldstein equation, the Doppler-shifted frequency remains constant while the intrinsic frequency varies with depth.

The long-time packet behavior differs from the solutions obtained by BB. In addition to $w'$, $u'$ and $E$ vanish in the limit of large time. While the vertical wavenumber and wave-induced shear increase, by the time they become sufficiently large to allow instability, $E$ is greatly reduced.

The cause of the difference is that, in this packet setup, the ray paths are not converging to a single critical-layer position, or even a critical-layer region that is narrow relative to the vertical dimension of the packet. Instead, lines of constant phase flatten uniformly in depth as $\omega'$ decreases. Ignoring packet edge effects, which do not alter the conclusions here, this absence of convergence reduces the equation for the action density A (see (5.8)) to $\partial A/\partial t = 0$ because there is only a minor gradient in $A$ or in the group velocity across the packet; accordingly, as $\omega'$ decreases, so must $E$.

A similar asymptotic behavior governs the decaying modes associated with the sudden start from rest in the BB investigation. Why these two limits should agree is explained physically by BB and mathematically by Brown & Stewartson (1980). An initial perturbation can be divided into a discrete spectrum, with finite energy in a mode of zero bandwidth, and a continuous spectrum. Given enough time, the disturbances in the continuous spectrum always decay in a constant-shear flow because each individual component selects its own critical layer. Any initial convergence ends as the rays (in a WKB sense) become more horizontal.

In Hartman's work, the decay is monotonic because of the initial conditions. These conditions might arise as the mean flow accelerates from zero velocity through a sequence of constant-shear profiles (Thorpe, 1978). If, on the other hand, a packet propagates from a motionless region into a shear layer, both $\delta\omega'/\omega'_c$ and $\delta\omega/\omega'_c$ are small. Since the spread in critical layers is also small, ray paths initially approach each other possibly producing large values of $E$ before decaying. It is therefore not just a continuous range, but a continuous and broad range of Doppler-shifted frequencies that differentiates Hartman's theory from the critical-layer theory of Bretherton (1966) and from those theories based on the Taylor-

Goldstein equation.

Although Hartman's analysis applies only to currents with constant shear, an important implication is not so restricted: the initial orientation of the rays can be as important as the structure of the currents for short wave dynamics.

An objective of Chapter 5 is to use ray theory to contrast the dissipation mechanisms reviewed in this chapter with the ways in which inertial currents refract short waves to unstable amplitudes. We also return to the subject of packet bandwidth in Chapter 5, Section C. The accuracy of ray theory is first discussed and tested in the following two chapters under the conditions observed in the deep ocean.

# CHAPTER 3

## SCALE ESTIMATES AND WKB ACCURACY

The analyses of Hartman (1975) and BB apply without restriction to slowly varying mean flows, but since the goal of this thesis is to incorporate inertial shears, which are neither steady nor constant in $z$, progress hinges more heavily on WKB techniques.

In this chapter and the next, an attempt is made to obtain some indication of WKB accuracy by confining attention to steady mean flows. The results of Hartman (1975) show negligible amounts of partial reflection and excellent agreement with WKB predictions. The estimates of vertical wavenumber agree exactly, since the equation

$$\frac{\partial m}{\partial t} = k\frac{\partial U}{\partial z} \tag{3.1}$$

holds whether the mean flow varies slowly or not. Action conservation also applies generally, but the action equation becomes approximate for the case studied by Hartman when $A$ is replaced by $E/\omega'$ (Andrews & McIntyre, 1978).

A further step toward validating WKB theory in the present context is to show that partial reflection is small when the dynamics are described by the Taylor-Goldstein equation. Wave properties then depend strongly on $z$ for typical oceanic conditions, as the following calculations illustrate.

If the shear is constant, the depth of the turning point $z_t$ is related to the depth of the critical layer $z_c$ by

$$z_t = z_c - Ri^{1/2}\frac{\lambda_x}{2\pi}\,, \tag{3.2}$$

where $\lambda_x = 2\pi/k$. Equation (3.2) is derived using $\omega = \omega' + Uk$, which may be rewritten as

$$\frac{\omega'}{N} = \frac{k(z_c - z)}{Ri^{1/2}}\,. \tag{3.3}$$

For $Ri \lesssim 10$, a distance of less than half a horizontal wavelength separates the turning point from the critical layer (in contrast with, for example, LeBlond and Mysak, 1978, figure 41.1).

Another measure of proximity, which is more pertinent to WKB accuracy, is the time required for a wave group to reach the critical layer. Within the WKB approximation this time is infinite, but by integrating along a ray to a level just below the critical layer where the

amplitudes and shears are large, a time scale shorter than a few Vaisala periods is predicted and confirmed by experiment (Thorpe, 1981; Koop, 1981).

When weighted by the local value of $\omega'$, the dimensionless propagation time $T_*$ becomes (for constant $U_z$)

$$T_* \equiv \int \omega' dt = \int_{z_i}^{z_c - z} \frac{\omega'}{C_{g3}} dz$$

$$= Ri^{1/2} \log \left[ \frac{Ri^{1/2}}{k(z_c - z)} + \left( \frac{Ri}{k^2 (z_c - z)^2} - 1 \right)^{1/2} \right] . \tag{3.4}$$

where $C_{g3}$ is the vertical component of the group velocity. A conservative choice of $k(z_c - z) = .1$ (see Thorpe, 1981, figure 2) and $Ri = 4$ yields the results $\omega'/N = .05$ (from (3.3)) and $T_* \cong 7$.

The effects of such rapid variation on WKB accuracy can be estimated by introducing the variable (Olver, 1974)

$$\xi = \int_{z_0}^{z} m(z') dz' , \tag{3.5}$$

where $m$ is the coefficient appearing in the Taylor-Goldstein equation, (2.1), and $z_0$ is an arbitrary depth. Substituting $\xi$ into the Taylor-Goldstein equation leaves

$$w_{\xi\xi} + w + \frac{1}{m^2} \frac{\partial m}{\partial z} w_\xi = 0 . \tag{3.6}$$

The WKB method attempts a solution for $w$ in terms of an asymptotic expansion. To leading order, $w$ is given by

$$w \sim \sqrt{\frac{m(z_0)}{m(z)}} \, e^{i\xi} \tag{3.7}$$

provided

$$\mu \sim O\left( \frac{1}{m^2} \frac{\partial m}{\partial z} \right) \ll 1 . \tag{3.8}$$

When the shear is constant, or the term $U_{zz}/(c - U)$ in $m$ is negligible, this becomes

$$\frac{1}{Ri^{1/2}} \frac{1}{\left( 1 - \frac{\omega'^2}{N^2} \right)^{3/2}} \ll 1 , \tag{3.9}$$

which is satisfied whenever $Ri$ is large except near turning points. A similar constraint on the Richardson number is derived by Hartman (1975).

The criterion (3.8) emphasizes that the validity of (3.7) depends on the fractional change in $m$, not m itself, and that the fractional change must be small over a distance of $1/m$, not a vertical wavelength. It can also be shown that the expansion is doubly asymptotic: the error approaches zero as $\mu \to 0$ for fixed $z$, or as $z \to z_0$ for fixed $\mu$ (Olver, 1974). Stated another way, the solution (3.7) is accurate through a nondimensionalized (by m) distance of the order of $1/\mu$. Since an infinite number of vertical wavelengths separate $z_0$ from the critical layer, the WKB approximation must eventually break down (Bretherton, 1966).

Judging from Sanford's measurements, the condition (3.9) may be violated frequently, even away from turning points. Because the solution for $w$ given by (3.7) is the first term in an asymptotic expansion, the result could be improved by working out higher order terms. If these terms are small relative to the first, it would be tempting to conclude that the first term alone is adequate; this reasoning may cause troubles, however, in dealing with reflection. Since the energy reflected by smooth changes in the medium is exponentially small as $\mu \to 0$, it never appears at any order in the expansion (Meyer, 1980). Higher order terms represent small changes in phase and amplitude but never generate, for example, downgoing waves from upgoing ones.

The process of comparing higher order terms to check the validity of the WKB method therefore has limitations. Only as $\mu \to 0$ is the error in an asymptotic expansion the order of the first term excluded. Partial reflection may account for the difference between a solution accurate asymptotically and a solution accurate for finite $\mu$.

# CHAPTER 4

# REFLECTION

## A. Theory

The circumstances in which a smooth velocity profile induces partial reflection are examined in this chapter by calculating exact solutions to the Taylor-Goldstein equation that can be interpreted as traveling waves as $z \to \pm\infty$. We choose as a convenient mean flow profile

$$U = U_0 \tanh \beta z \,, \tag{4.1}$$

for which the Taylor-Goldstein equation is

$$w_{zz} + \left\{ \frac{N^2}{(c-U)^2} - \frac{2\beta^2 U(1-U^2)}{c-U} - k^2 \right\} w = 0 \,. \tag{4.2}$$

Introducing the dimensionless quantities

$$U_* = \frac{U}{U_0} \,, \quad c_* = \frac{c}{U_0} \,, \quad J = \frac{N^2}{\beta^2 U_0^2} \,, \quad \alpha = \frac{k}{\beta}$$

and transforming the dependent variable from $z$ to $U_*$ turns (4.2) into a Fuchsian equation with four singular points:

$$w_{U_*U_*} - \frac{2U_*}{1-U_*^2} w_{U_*} + \left\{ \frac{J}{(c_*-U_*)^2(1-U_*^2)^2} - \frac{2U_*}{(c_*-U_*)(1-U_*^2)} - \frac{\alpha^2}{(1-U_*^2)^2} \right\} w = 0 \,. \tag{4.3}$$

The singularities are located at $U_* = -1$, 1, $c_*$, and $\infty$. Any equation with four regular singular points can be transformed to Heun's equation by a two step procedure. The first step is to bring the singularity at $U_* = -1$ to $U_* = 0$ so that three of the singularities are at 0, 1, and $\infty$. This is achieved through the transformation

$$U_1 = \frac{(U_*+1)}{2} \,.$$

Defining

$$c_1 = \frac{(c_*+1)}{2} ,$$

equation (4.3) becomes

$$w_{U_1U_1} + \left\{\frac{1}{U_1} + \frac{1}{U_1-1}\right\} w_{U_1} + \left\{\frac{1}{U_1}\left[\frac{J}{16c_1} - \frac{\alpha^2}{4}c_1\right] + \right.$$

$$\left. \frac{1}{U_1-1}\left[\frac{J}{16(1-c_1)} - \frac{\alpha^2(1-c_1)}{4}\right] - \frac{1}{(U_1-c_1)}\left[\frac{J}{16c_1(1-c_1)}\right] - 2U_1 + 1\right\} w = 0 . \tag{4.4}$$

The solution to (4.4) is represented by the Riemann symbol

$$w = P\begin{Bmatrix} 0 & 1 & c_1 & \infty & \\ i\mu_1 & i\mu_2 & \tfrac{1}{2}(1+i\nu) & 2 & U_1 \\ -i\mu_1 & -i\mu_2 & \tfrac{1}{2}(1-i\nu) & -1 & \end{Bmatrix} , \tag{4.5}$$

where

$$\mu_1 = \frac{1}{2}\left\{\frac{J}{4c_1^2} - \alpha^2\right\}^{1/2} \tag{4.5a}$$

$$\mu_2 = \frac{1}{2}\left\{\frac{J}{4(1-c_1)^2} - \alpha^2\right\}^{1/2} \tag{4.5b}$$

$$\nu = \left\{\frac{J}{4c_1^2(1-c_1)^2} - 1\right\}^{1/2} . \tag{4.5c}$$

The exponents of (4.5) govern the behavior of the solution at each of the singular points. For example, if $A$ and $B$ are complex constants, then

$$w \sim AU_1^{i\mu_1} + BU_1^{-i\mu_1}$$

$$= Ae^{i\mu_1 \ln U_1} + Be^{-i\mu_1 \ln U_1}$$

as $U_1 \to 0$. In this limit

$$\frac{\partial}{\partial z}\mu_1 \ln U_1 = \mu_1 ,$$

so $\mu_1$ is identified as the dimensionless vertical wavenumber as $z \to -\infty$. Similarly, $\mu_2$ corresponds to the dimensionless vertical wavenumber as $z \to +\infty$.

The second step in putting (4.3) in the form of Heun's equation requires a transformation of the dependent variable $w$ by

$$w_1 = U_1^{-i\mu_1}(U_1-1)^{-i\mu_2}(U_1-c_1)^{-\frac{1}{2}(1+i\nu)}w \,. \tag{4.7}$$

Inserting this into (4.4) leaves

$$w_{1_{U_1U_1}} + \left\{\frac{\gamma}{U_1} - \frac{\nu+2\mu_1+2\mu_2+3}{U_1-1} + \frac{\delta}{U_1-c_1}\right\}w_{1_{U_1}} + \frac{\bar{\alpha}\bar{\beta}U_1-b}{U_1(U_1-1)(U_1-c_1)}w_1 = 0 \,, \tag{4.8}$$

where

$$\bar{\alpha} = \frac{5}{2} + i\mu_1 + i\mu_2 + \frac{i\nu}{2} \,, \tag{4.9}$$

$$\bar{\beta} = -\tfrac{1}{2} + i\mu_1 + i\mu_2 + \frac{i\nu}{2} \,, \tag{4.10}$$

$$\gamma = 1 + 2i\mu_1 \,, \tag{4.11}$$

$$\delta = 1 + i\nu \tag{4.12}$$

and

$$b = 1 + (\mu_1^2-\mu_2^2) + c_1(\mu_1^2+\mu_2^2-i(\mu_1+\mu_2)) - \tfrac{1}{2}(1+i\nu)(1+i\mu_1+\tfrac{1}{2}(1-i\nu)(c_1-1)) \,. \tag{4.13}$$

(In defining the parameters in (4.9) to (4.13), The notation of Snow (1942) is followed as closely as possible.) The Riemann symbol is now

$$w_1 = P\begin{Bmatrix} 0 & 1 & c_1 & \infty & \\ 0 & 0 & 0 & \bar{\alpha} & U_1 \\ -2i\mu_1 & -2i\mu_2 & -i\nu & \bar{\beta} & \end{Bmatrix} \tag{4.14}$$

Equation (4.8) is Heun's equation. That solution which is analytic at $U_1$=0 (i.e. has zero exponent) is known as Heun's function and is given by the series

$$F(c_1,b;\bar{\alpha},\bar{\beta},\gamma,\delta;U_1) = \sum_{n=0}^{\infty} a_n U_1^n \,. \tag{4.15}$$

A three-term recursion formula determines the $a_n$'s:

$$a_0 = 1\,, \quad a_1 = \frac{-b}{\gamma c_1}$$

and

$$a_{n+2}(n+1+\gamma)c_1 =$$

$$a_{n+1}\Big\{(n+1)^2(1+c_1) + (n+1)(\gamma+\delta-1+(\bar{\alpha}+\bar{\beta}-\delta)c_1-b)\Big\} - a_n(n+\bar{\alpha})(n+\bar{\beta}) \tag{4.16}$$

Drazin (1958) derives an equation similar to (4.8) with $c = 0$ to study shear instability (see equation (23) of Drazin's paper). Drazin notes that if $w_1$ is constant, a solution that satisfies the boundary condition of $w_1 \to 0$ as $z \to \pm\infty$ is obtained if

$$\bar{\alpha}\bar{\beta}U_1 - b = 0\,. \tag{4.17}$$

In Drazin's problem, $b$ is zero and $\bar{\alpha}$ can never vanish, so, by equating $\bar{\beta}$ to zero, the singular neutral curve

$$J = \alpha^2(1-\alpha^2) \tag{4.18}$$

is found.

Here we seek solutions to (4.8) that represent an incident plus a reflected wave as $z \to -\infty$ $(U_1 \to 0)$

$$w(z) = e^{-i\mu_1\beta z} + \mathrm{Re}^{i\mu_1\beta z}\,, \tag{4.19}$$

and a transmitted wave as $z \to +\infty$ $(U_1 \to 1)$

$$w(z) = Te^{-i\mu_2\beta z}\,. \tag{4.20}$$

The amplitude of the incident wave in (4.19) has been set equal to unity, and the complex constants $R$ and $T$ are related to the fractional reflected and transmitted energy densities by

$$E_R = |R|^2 \tag{4.21}$$

$$E_T = |T|^2\,\frac{(\alpha^2+\mu_2{}^2)}{(\alpha^2+\mu_1{}^2)}\,. \tag{4.22}$$

The analytical continuation formulae necessary to determine $R$ and $T$ are given in Appendix A; however, the resulting expressions (A4) and (A5) in terms of Heun's functions are not very useful. A simpler and more interpretable form can be derived if the number of singularities in (4.3) can be decreased by one, because Heun's equation then reduces to a hypergeometric equation. One way to accomplish this, valid in the limit of $J \to \infty$ or $c \downarrow U_0$, is to ignore the $U_{zz}$ term in the Taylor-Goldstein equation, which is responsible for the singularity as $U_z \to \infty$. Under this assumption, the equation for $|R|$ derived by van Duin & Kelder (1982) and converted to the present notation is

$$|R|^2 = \frac{\cosh^2(\frac{\pi\nu}{2}) + \sinh^2\pi(\mu_2-\mu_1)}{\cosh^2(\frac{\pi\nu}{2}) + \sinh^2\pi(\mu_2+\mu_1)} . \tag{4.23}$$

**B. Discussion**

Two limiting forms of (4.23) follow easily. The first is the limit of large Richardson number. If this is achieved by letting $N \to \infty$ or $\beta \to 0$, then $\mu_1$, $\mu_2$, and $\nu$ tend to infinity, leaving the approximate solution

$$|R| = e^{-2\pi\mu_1} \tag{4.24}$$

(van Duin & Kelder, 1982). If instead, the Richardson number is increased by letting $U_0 \to 0$, (4.24) still holds provided a short-wavelength approximation, $2\pi\mu_1 >> 1$, is made. This case illustrates the exponentially small magnitude of the reflected energy in the WKB limit, as mentioned in Chapter 3.

The second limit of interest is $c \downarrow U_0$. By again imposing $2\pi\mu_1 >> 1$, the relationship (4.24) is obtained. Partial reflection is therefore unimportant for waves that just miss satisfying critical-layer conditions. Mied & Dugan (1975) reach the same conclusion from a numerical integration of the Taylor-Goldstein equation.

When a critical layer exists within the shear layer, partial reflection is again unimportant, except at low Richardson number, where waves may be overreflected. BB attribute the reflected energy appearing in their results not to partial reflection, but to reflection from the discontinuity in their velocity profile. This energy is derived from waves that pass through the critical layer twice, once before and once after reflection. Each time the energy flux is diminished by an exponential factor (the BB transmission coefficient), yet the discontinuity still accounts for the major portion of reflected energy.

It is of interest to see whether a symmetric profile produces the same behavior. One such profile that approaches constant values as $z \to \pm\infty$ is $U = U_0 sech^2(\beta z)$. The resulting Taylor-Goldstein equation can be transformed into a Fuchsian one by the same change of variable, $V = \tanh(\beta z)$, that is used for the tanh profile. Here, though, the number of singularities increases to five (except when $c = U_0$ which leads to one irregular and three regular singular points.) Rather than proceeding by the method outlined in Appendix B, it is simpler to model the entire coefficient of the Taylor-Goldstein equation

$$m^2 \equiv \frac{N^2}{(c-U)^2} + \frac{U_{zz}}{(c-U)} - k^2 \tag{4.25a}$$

by

$$m^2 = A + B sech^2(\beta z) \tag{4.25b}$$

with $A, B > 0$ (Epstein, 1930). Neglecting the term $U_{zz}/(c-U)$ in (4.25a) we can solve for U to obtain

$$U = c - \frac{N}{(k^2 + A + B sech^2 \beta z)^{1/2}} \tag{4.26}$$

The form of the reflection coefficient depends on the nature and position of the zeros and singularities of $m^2$ (Meyer, 1980). For the model (4.25) to be appropriate, the zeros must resemble classical turning points and the singularities must resemble critical layers. The coefficient $m$ vanishes at

$$z = \frac{(-i\pi)}{2} \pm \log\left(\frac{A}{2B+A}\right) \tag{4.27}$$

while the singularities of $m$ lie at $z = \pm i\pi/\beta$. A Taylor expansion verifies that the proper limits result: $m^2$ has simple zeros, and its only singularities are second order poles. (Note that the antisymmetric model of Epstein (1930), $m^2 = A + B\tanh(\beta z)$ gives a first order pole at the singularity and is therefore inappropriate for a stratified shear flow; it is pertinent, however, to unstratified problems, including Rossby wave - mean flow interactions.)

Epstein obtains

$$|R|^2 = \frac{\sin^2(\pi d)}{\sin^2(\pi d) + \sinh^2\left(\pi \frac{A^{1/2}}{\beta}\right)} \tag{4.28}$$

for the reflection coefficient, where

$$d = 1/2 - 1/2(1 + B/\beta^2)^{1/2} \tag{4.29}$$

and

$$a = A^{1/2}/\beta \,. \tag{4.30}$$

For the three cases

(i) $\beta \to 0$,

(ii) $B \to 0$, $\pi A^{1/2}/\beta >> 1$, and

(iii) $B \to \infty$

$|R|$ takes the approximate form

$$|R| = \sin(\pi d) e^{-2\pi A^{1/2}/\beta} \,. \tag{4.31}$$

The first two limits correspond to $Ri \to \infty$ and the last limit to $c \to U_0$. As for the case $U = U_0 \tanh(\beta z)$, the reflected energy is exponentially small for waves that have phase speeds barely exceeding the mean flow maximum.

A final remark concerns the validity of the WKB approximation. Although partial reflection does not impair the accuracy of WKB solutions in the limit of $J \to \infty$ or $c \downarrow U_0$, WKB approximations fail when applied to a curved velocity profile with low Richardson number. Then the term $U_{zz}/(c-U)$ dominates the others in the coefficient of the Taylor-Goldstein equation. An example depicting the importance of this term for a tanh velocity profile is plotted in figure 4.1. Within the WKB approximation, $m^2$ increases monotonically with depth because the shear is always positive, but what the approximation predicts to be refraction toward low frequency turns out to be refraction toward a turning point, since the exact value of $m^2$ becomes negative where the curvature term gains influence. It appears that this concern and not partial reflection is the major drawback in applying WKB techniques to flows described by the Taylor-Goldstein model.

However, the application of the Taylor-Goldstein model to short waves in inertial currents has severe limitations, since the approximation of steady shears is valid only for times that are short relative to an inertial period. (Note that in the results of figure 1.1, the time dependence of the currents becomes important before one-tenth of an inertial period has elapsed.) This restricts the model's utility to waves of high intrinsic frequency. Another factor enters though: the vertical gradient in the Doppler-shifted frequency $\omega$. If this gradient is large, as in the problem of Hartman (1975), the Taylor-Goldstein model is inappropriate even for short times.

Nevertheless, the Taylor-Goldstein equation is useful in testing WKB accuracy. It provides the Richardson number criterion given in (3.9) and an indication of the importance, or unimportance, of partial reflection. Such results are difficult to obtain from analyses that include

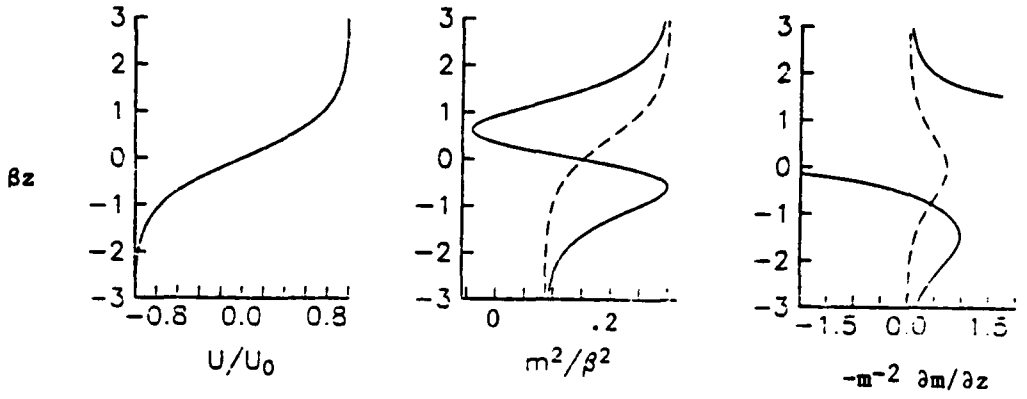


Figure 4.1. The coefficient of the Taylor-Goldstein equation. The asymptotic predicitions (dashed lines), obtained by neglecting the curvature term $U_{zz}/(c-U)$ in the Taylor-Goldstein equation, are compared with the exact values (bold lines). The calculations are made for $J=2.0$, $c/U_0=3.0$, $(\omega'/N)_{-\infty}=.3$, and $k/\beta=.1$. Asymptotic theory does not anticipate the turning point just above $\beta z=0$.

time-varying shears, although some progress along these lines can be made by extending Hartman's theory to a time-dependent current of the form $U_z = U_z(t \text{ only})$ (Thorpe, 1978).

# CHAPTER 5

## SHORT-WAVE PROPAGATION IN AN INERTIAL CURRENT

Large-amplitude inertial oscillations with vertical wavelengths of a few hundred meters or less are found wherever measurements are made in the ocean. They constitute the major shear throughout the water column, strongly refracting short waves and creating the possibility for short-wave —— critical-layer interactions.

The effects of inertial currents on the propagation of short waves and on the evolution of critical-layer encounters are analyzed here using ray theory. Strictly speaking, the introduction of time-varying shears eliminates singularities associated with critical layers; at issue, however, is whether behavior resembling the BB predictions can still be achieved and, if so, which conditions favor its occurrence.

Rotation, which has previously been ignored, is introduced in this chapter. Jones (1967) analyzes the critical-layer interaction by modifying the Taylor-Goldstein equation to include rotation. He finds that rotation introduces two additional singularities at the depths at which $\omega' = \pm f$, where $\omega'$ and $f$ are the intrinsic and inertial frequencies respectively. He also finds an exponential decrease in the vertical flux of horizontal pseudomomentum (Andrews & McIntyre, 1978) across the singularity at $\omega' = f$. However, the result most relevant to the present purposes is that, in a rotating fluid, critical-layer convergence and the shear instability predicted by Hartman (1975) occur as $\omega' \rightarrow f$. (In Hartman's theory, this is a WKB result, since $\omega'$ is meaningfully defined in his analysis only in the WKB limit.)

We take as a simple model of an inertial current the standing wave

$$\mathbf{U} = (U,V,0) = U_0 \sin\beta z\,(\sin ft, \cos ft, 0) \tag{5.1}$$

with wavelength $\lambda_i = 2\pi/\beta$ and period $T_i = 2\pi/f$, We consider short waves of wavenumber $\mathbf{K} = (k,0,m)$ and assume that the short-wave amplitudes are independent of horizontal position. Then the $y$—component of the inertial velocity $V$ does not enter into the ray equations and therefore need not be considered in the following calculations.

The short waves have intrinsic frequency $\omega'$, Doppler-shifted frequency $\omega$, and since $k$ is assumed positive,

$$\omega = \omega' + Uk \quad . \tag{5.2}$$

The group velocity of the short waves is $\mathbf{C}_g = (C_{g1},0,C_{g3})$, with

$$C_{g1} = \frac{1}{\omega' k}\left(\frac{\omega'^2 - f^2}{N^2 - f^2}\right)(N^2 - \omega'^2) \tag{5.3a}$$

$$C_{g3} = -\tfrac{1}{2}\frac{(N^2 - f^2)}{\omega'}\,\frac{k^2 m}{(k^2+m^2)^2}\,, \tag{5.3b}$$

and as in previous chapters, $c'$ and $c$ are the intrinsic and Doppler-shifted horizontal phase speeds respectively.

The minimum Richardson number of the inertial current, $J$, and $N/f$ are set to

$$J = \frac{N^2}{\beta^2 U_0^2} = 4\,, \qquad \frac{N}{f} = 50\,. \tag{5.4a,b}$$

The magnitude of $J$ represents a compromise between the measured values of Sanford (1975, figure 12), which fall within 1 and 4 ninety percent of the time, and concerns for WKB accuracy (see (3.9)). The value for $N/f$ is appropriate to a depth of roughly 1000 meters at midlatitudes.

## A. Ray Theory

Writing the dispersion relation as

$$\omega(z,t) = \Omega(\mathbf{K},z,t) = \left(\frac{k^2N^2 + m^2f^2}{k^2+m^2}\right)^{1/2} + kU \tag{5.5}$$

the equations to be integrated along rays defined by

$$\frac{d\mathbf{x}}{dt} = \mathbf{C}g + \mathbf{U}\,, \qquad \frac{d}{dt} = \frac{\partial}{\partial t} + (\mathbf{C}g + \mathbf{U})\frac{\partial}{\partial \mathbf{x}} \tag{5.6a,b}$$

are (Garrett, 1968)

$$\frac{d\omega}{dt} = k\frac{\partial U}{dt} \tag{5.7}$$

$$\frac{dA}{dt} = -A\frac{\partial}{\partial z}C_{g3}$$

$$= -A\left(\frac{\partial m}{\partial z}\Omega_{mm} + \Omega_{mz}\right), \tag{5.8}$$

where $A$ is the wave action density. We have adopted the notation of Hayes (1970), using $\Omega$ and denoting partial derivatives by subscripts when the independent variables include $\mathbf{K}$ as well as $z$ and $t$. The variable $x$ enters only in the equation for the $x$–component of the ray path.

In all other equations, $d/dt$ can be reduced to $\partial/\partial t + C_{g3}\partial/\partial z$.

Rather than integrating along adjacent rays to determine $\partial m/\partial z$ in (5.8), Hayes suggests advecting the value of $\partial m/\partial z$ along the single ray defined by (5.6). This introduces another equation

$$\frac{d}{dt}\left(\frac{\partial m}{\partial z}\right) = -\Omega_{zz} - 2\frac{\partial m}{\partial z}\,\Omega_{zm} - \left(\frac{\partial m}{\partial z}\right)^2 \Omega_{mm} \tag{5.9}$$

(see Hayes (1970), equation (19)). From the dispersion relation, we find that

$$\Omega_{zm} = 0\,, \tag{5.10a}$$

$$\Omega_{zz} = k\frac{\partial^2 U}{\partial z^2}\,, \tag{5.10b}$$

$$\Omega_{mm} = k^2(f^2-N^2)(a^{-1/2}b^{-3/2})\left[1 - m^2(3b^{-1} + N^2a^{-1})\right]\,, \tag{5.10c}$$

where in (5.10c)

$$a = k^2N^2 + m^2f^2 \tag{5.10d}$$

$$b = k^2 + m^2\,. \tag{5.10e}$$

From $A$, we compute the intrinsic energy density $E$, which is given by

$$E = \frac{\rho_0}{2}\,\overline{(u'^2 + v'^2 + w'^2 + \theta'^2/N^2)} \tag{5.11}$$

$$= A\,\omega' \tag{5.12}$$

and which satisfies the ray equation

$$\frac{dE}{dt} = E\,\frac{\partial}{\partial z}C_{g3} + \frac{1}{\omega}\,\frac{d\omega'}{dt} \tag{5.13}$$

It marks the energy density measured by an observer moving with the local velocity of the mean current.

We also compute the pseudoenergy density $e$, related to $A$ and $E$ in the WKB limit by

$$e = \omega\,A = \omega\,\frac{E}{\omega}, \tag{5.14}$$

The ray equation for $e$

$$\frac{de}{dt} = e\,\frac{\partial}{\partial z}C_{g3} + \frac{1}{\omega}\,\frac{d\omega}{dt} \tag{5.15}$$

shows that $e$ is conserved whenever $\omega$ is constant along the ray, or equivalently, whenever the medium is time independent.

In the results presented in this chapter, $E$ is emphasized over the quantities $A$ and $e$ because it provides the best indication of whether or not the waves reach large amplitudes. In this respect, $A$ has the disadvantage of reflecting changes in $\omega'$ in addition to amplitude. In the case studied by Hartman (1975), for example, $A$ remains constant as the wave amplitudes grow or decay. A similar concern holds for $e$, which may even be zero or negative.

To calculate the exact Richardson number as a function of time and depth, the amplitude and phase of the short waves must be specified. If $u'$ and $v'$ are the horizontal perturbation velocities and $\rho'$ the perturbation density, the Richardson number can be expressed as

$$Ri = \frac{N^2 + \frac{g}{\rho_0}\frac{\partial \rho'}{\partial z}}{\left[\frac{\partial}{\partial z}(U+u')\right]^2 + \left[\frac{\partial}{\partial z}(V+v')\right]^2} . \tag{5.16}$$

Letting $u' = u_0 \cos\phi$, (5.16) becomes

$$Ri = \frac{\frac{J}{(\cos\beta z)^2}\left[1 + \frac{1}{f^{\prime 2}}\gamma\cos\phi\right]}{1 + 2\gamma(\cos\phi\sin ft + \frac{f}{\omega'}\sin\phi\cos ft) + \gamma^2(\sin^2\phi + \frac{f^2}{\omega'^2}\cos^2\phi)} . \tag{5.17}$$

where

$$\gamma = \frac{u_0}{c'}\frac{c'}{U_0}\frac{m}{\beta}\frac{1}{\cos\beta z} . \tag{5.18}$$

The quantity, $u_0/c'$, is set to .2 at the initial coordinates and computed at later times from the WKB relationship

$$E = \tfrac{1}{4}\rho_0 u_0^2\left\{1 + \frac{f^2}{\omega'^2} + \frac{k^2}{m^2}\left[1 + \frac{N^2}{\omega'^2}\right]\right\} , \tag{5.19}$$

with $E$ obtained from the solution for wave action, (5.8). The minimum and maximum Richardson numbers are determined by running through 50 values of $\phi$ at each time-step.

Equations (5.6)-(5.9) are integrated using the variable-order method of Bulirsch and Stoer (1966). As a check, the formula for the intrinsic frequency is included:

$$\frac{d\omega'}{dt} = -kC_{g3}\frac{\partial U}{\partial z} . \tag{5.20}$$

The integration ends if $E$ exceeds 50 times its initial magnitude or if $Ri < 1/4$. We shall refer to this process, by which unstably high amplitudes are attained, as a focussing or convergence. Once started, focussing typically proceeds at a rapid rate, so the final values of $\omega$, $\mathbf{x}$, and $t$ are seldom sensitive to the cutoff value for $E$. In addition, the focussing of rays is the sole cause of instability in all cases presented in this chapter: examples of shear intensification in which the rays remain parallel, as envisioned by Hartman (1975) and Phillips (1966) for steady, linear, mean flows, were never found.

**B. Results**

In figure 5.1, a ray calculation begins at $z = 0$, $t = 0$ with a Doppler-shifted, horizontal phase speed of $.6U_0$. The ray path would head asymptotically toward a critical layer near $z = .1\lambda_i$ if the mean flow was steady and maintained at $U = U_0 \sin(\beta z)$.

Instead, as the short waves propagate upward, the inertial wave accelerates causing $c/U_0$ to double from .6 to about 1.2 (figure 5.1b). At the same time, refraction reduces the intrinsic frequency to less than $2f$ (figure 5.1c). Despite the increase in vertical wavenumber (figure 5.1d), there is no tendency for shear instability (figure 5.1j) because the intrinsic energy density $E$ is greatly reduced (figure 5.1h) and because the mean shear is low near the level of one-quarter inertial wavelength.

Since internal waves of low frequency and high wavenumber propagate with small group velocity, vertical progress is slowed. Caught in the region of maximum currents, they are swept backwards in the decelerating phase of the inertial oscillation (figure 5.1a). A full inertial period elapses without any sign of instability or wave growth. It is not until the waves begin to emerge from the region of maximum currents that $E$ intensifies (reaching 50 times its initial value before the calculation is stopped); however, at this time, the intrinsic frequency and group velocity are *increasing* (figure 5.1c), which means that refraction is in a direction opposite to that required for a critical-layer interaction. The strong, time-dependent shears have therefore focussed an *accelerating* group of short waves to unstable amplitudes at a depth where critical-layer conditions are not satisfied.

The ability of inertial currents to focus short-wave groups that are accelerating will appear in many of the results presented in this chapter. It is a type of convergence seldom considered by steady-shear analyses. The reason is that these steady analyses generally assume or lead to solutions in which the Doppler-shifted frequency $\omega$ is independent of depth. Examples include the study of waves generated by flow over topography or by shear instability. In the steady-state case, with $\omega$ constant, the ray equation for $A$ takes the simple form, $AC_{g3} = constant$, so $A$ intensifies only as the wave group decelerates.

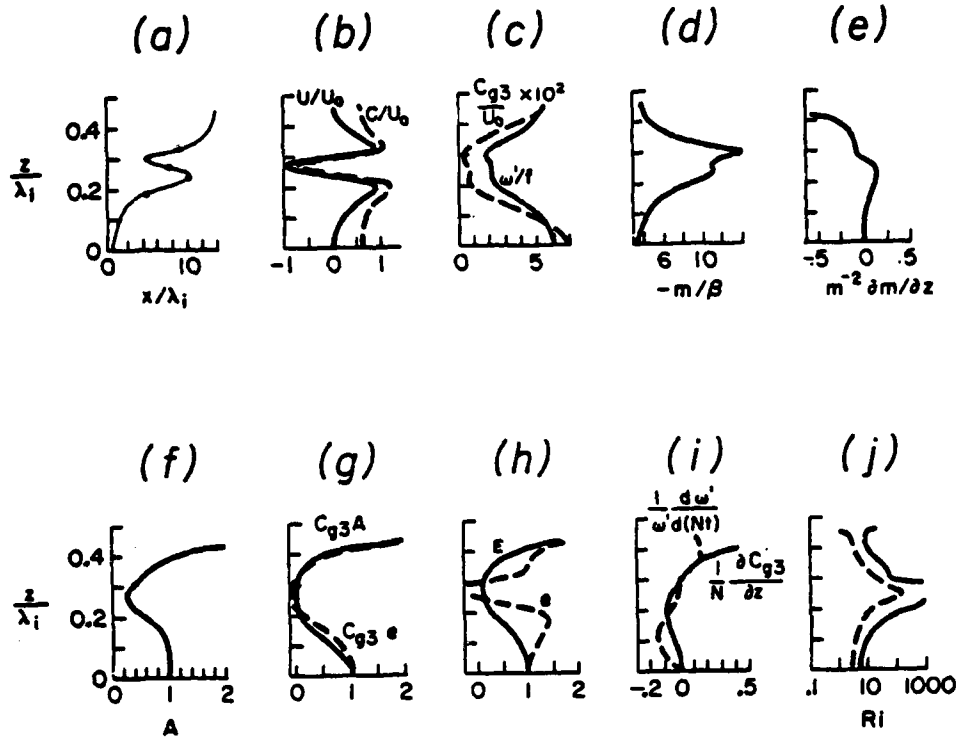


Figure 5.1. Summary of a ray-tracing integration for short waves propagating through an inertial current given by (5.1). All plots have the same vertical axis. At the initial time, $t=0$, $\omega'/f=6$, and $c/U_0=.6$ Time is marked parametrically in $(a)$ by dots along the ray path every quarter-inertial period. Minimum and maximum Richardson numbers (computed from (5.17)) are shown in $(j)$ by dashed and bold lines respectively. In addition to the graphs referenced in the text, the following are included:

- $(e)$ $m^{-2}\partial m/\partial z$, provided as an indication of WKB accuracy,
- $(g)$ the vertical fluxes of $A$ and $e$, and
- $(i)$ the terms contributing to changes in $E$ (see (5.13)).

Note that convergence takes nearly 1½ inertial periods to occur, and that at this time, $\omega'$ and $Cg_3$ are increasing.

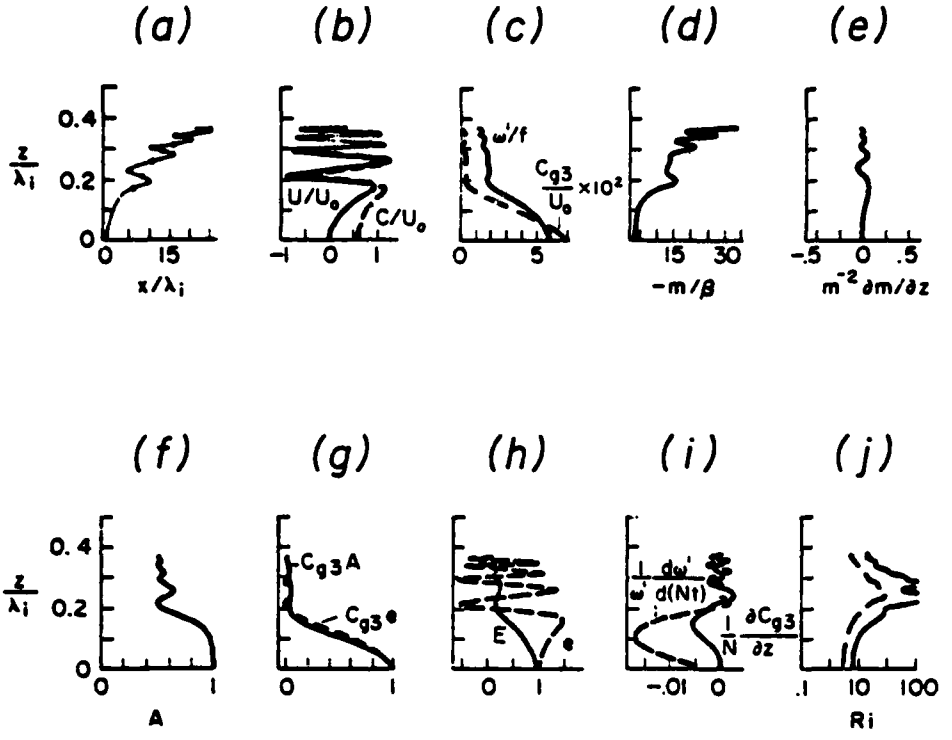


Figure 5.2. Same as for figure 5.1 except that a steady mean current has been added to the inertial oscilllation. The total background velocity in the $x$−direction is: $U=U_0\sin\beta z\sin ft+rz$, where $r^2=.001N^2$.

In the example pictured in figure 5.2, all the initial conditions are the same as in figure 5.1, except that a linear, steady mean flow of the form $U_l = rz$ has been added to the inertial-wave background. This is intended to model the shear of a geostrophic current or mesoscale eddy. The parameter $r$ is chosen such that the Richardson number of the steady flow is 1000, but the results are similar for a Richardson number of 100.

With this modification, the waves are refracted to small vertical wavelengths, but there is no tendency towards shear instability such as that which develops within a few Vaisala periods in Hartman's results. The Richardson number never gets near one-quarter, in part because of the curvature of the velocity profile and in part because $\partial U/\partial z$ vanishes twice every inertial period. The short waves are carried back and forth by the currents for nearly four inertial periods.

Unlike the previous two cases, short waves originating near the depth $z = .5\lambda_i$ find conditions resembling those of critical-layer interactions (figures 1.1, 5.3). These waves encounter a decelerating mean flow with positive shear ($\partial U/\partial z > 0$), similar to the situation in which Thorpe (1981) generates critical layers.

Despite an initial short-wave phase speed of $2U_0$, the convergence of ray paths shown in figure 5.3 develops well before the inertial current attains its maximum velocity, and convergence continues at depths where the shear becomes negative and thus where critical-layer conditions cannot be met; moreover, for the calculations summarized in figure 5.3, the value of $c$ is greater than $2U_0$ at the time of focussing and is therefore more than twice the local value of $U$.

That critical layers need not account for the majority of convergences predicted by ray theory is emphasized by figure 5.4, which summarizes the results of 576 sets of ray-calculations. (The symmetry $U(z,t) = U(z + \lambda_i/2, t + T_i/2)$ for $U$ given by (5.1) reduces the number of independent cases by a factor of two.) The initial conditions cover twelve times evenly spaced over an inertial period, twelve depths evenly spaced over an inertial wavelength, and four intrinsic phase speeds: $c'/U_0 = .2, .6, 1.0$, and 1.4. The initial intrinsic frequency is held fixed at $\omega' = .2$. Each integration continues for two inertial periods or two inertial wavelengths unless convergence causes the intrinsic energy density $E$ to intensify (see the final paragraph of section 5A). If this occurs, the integration stops and the final time and depth relative to the phase of the inertial oscillation are marked in the figure.

The shear is positive at the times and depths falling in the hatched sections of the plot. Although critical-layer interactions are restricted to this area, to classify all the cases in the hatched sections as critical-layer interactions is to include behavior that differs substantially from the results of BB and Thorpe (1981): sudden increases in $E$ occur at intrinsic frequencies

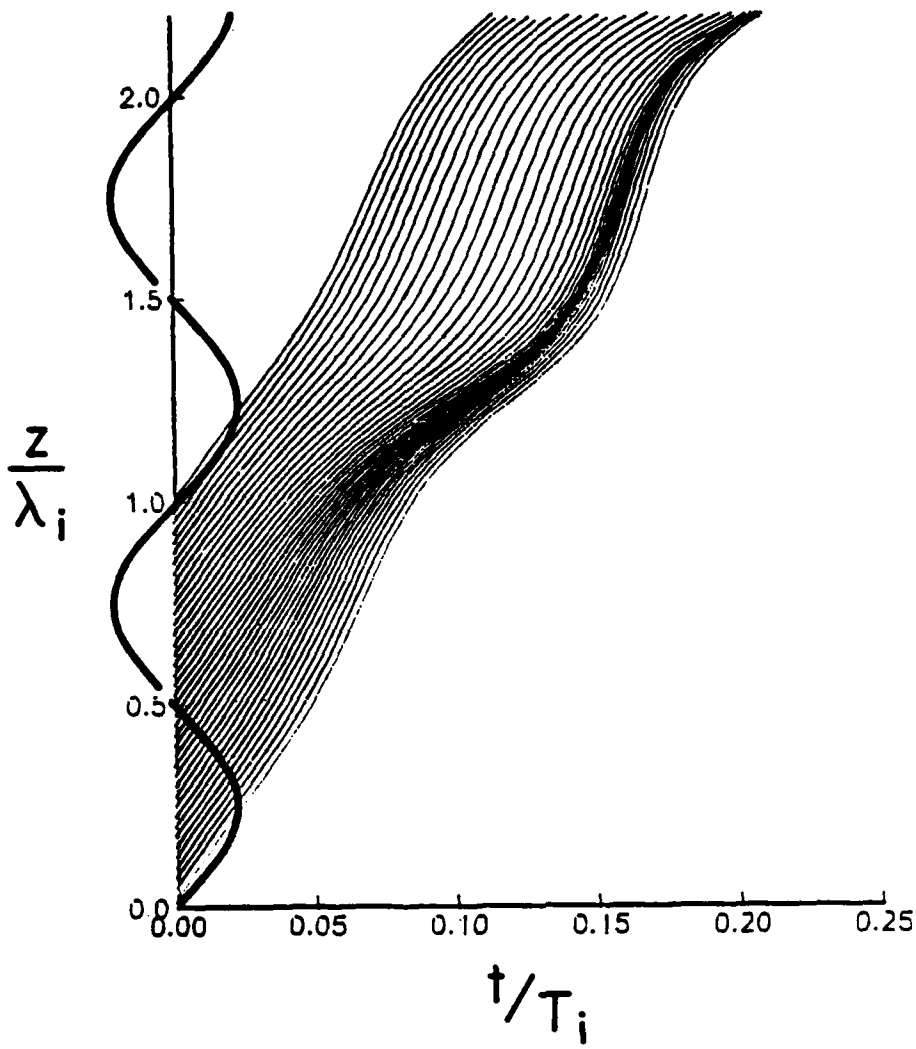


Figure 5.3. Ray trajectories in an inertial current given by (5.1). At $t=0$, $c/U_0=2.0$, $k/\beta=.2$, and $\omega'/N=.2$ The dark band extends through regions of positive and negative shear and represents a convergence band where 13 of the 40 initial rays terminate. The value of $U$ increases from zero at $t=0$ to the profile shown on the vertical axis at $t=.25T_i$.

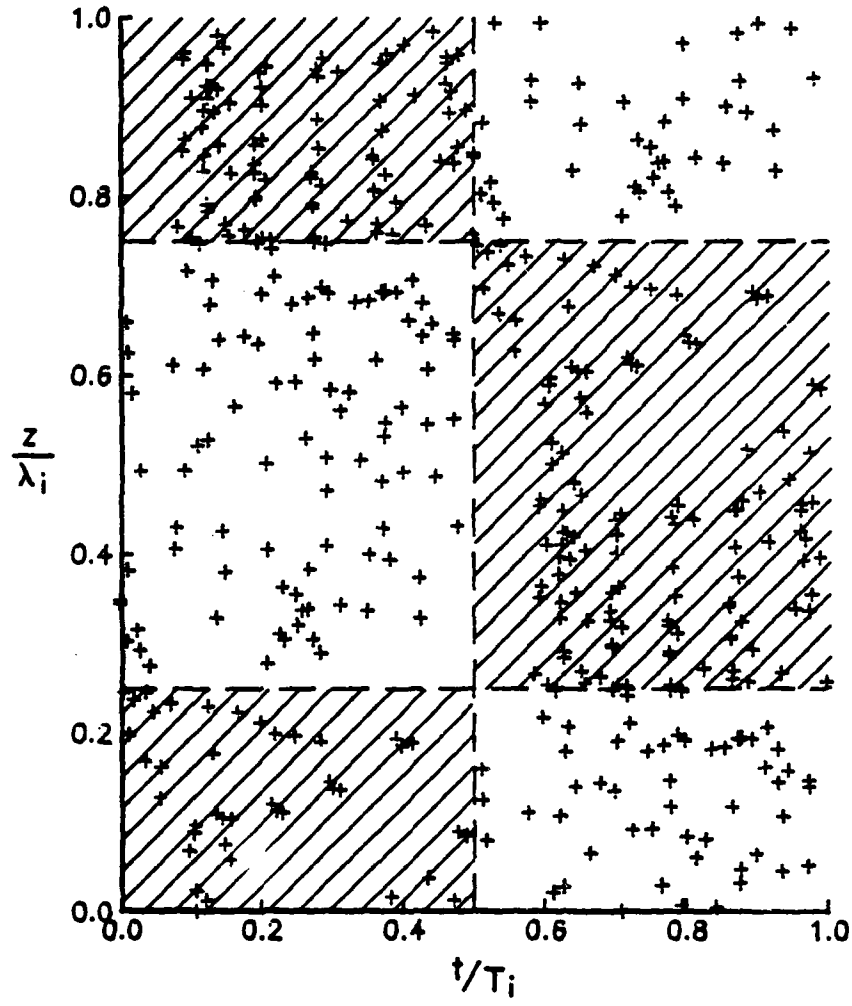


Figure 5.4. The location of convergences. Plus marks indicate the depth relative to an inertial wavelength $\lambda_i$, and the time relative relative to an inertial period $T_i$, at which the ray calculations predict convergence ($E>50E(t=0)$ or $Ri<¼$). The figure displays only the phase of the inertial current at which this happens. A ray which reaches $t=1.5T_i$ and $z=1.75\lambda_i$, for example, is given the coordinates (.5,.7). Cases in which the short waves propagate for longer than two inertial periods or two inertial wavelengths without becoming focussed are not plotted. The initial values of $c'/U_0$ are .2, .6, 1.0, and 1.4. Of 576 cases, 434 points are plotted (75% of the total) with 246 points falling in the hatched region, where critical-layer interactions are possible.

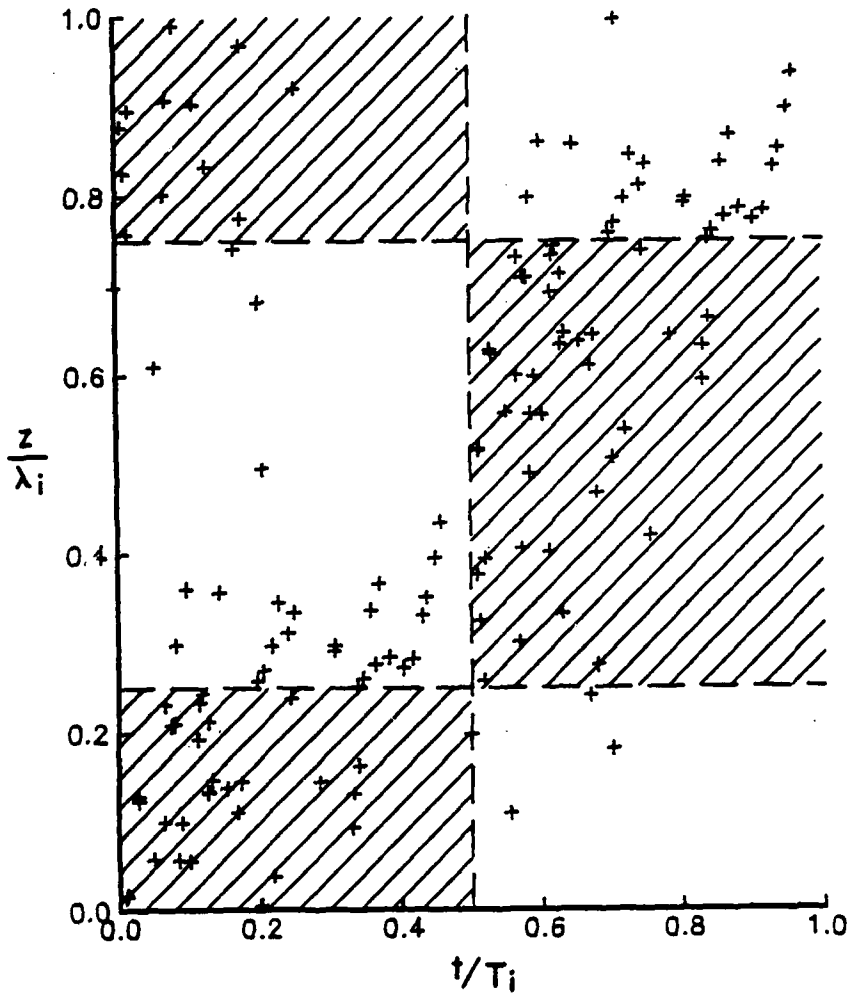


Figure 5.5. Same as for figure 5.4, except that the initial values of $c'/U_0$ are larger, ranging from 1.8 to 3.0. Of 576 cases, 138 points are plotted (24% of the total) with 83 points falling in the hatched sections.

much greater than $f$, at times when the current is weak everywhere, and at depths where the mean shear vanishes.

The number of cases that can be attributed to a critical-layer interaction depends on its definition. Let a critical-layer interaction be one in which wave amplitudes intensity as $\omega' \rightarrow f$ and, in the WKB approximation, as $C_{g3} \rightarrow 0$. Then only 10% of the cases plotted in figure 5.4 fit this definition if by $\omega' \rightarrow f$, we mean that $\omega' < 5f$ when focussing occurs. This increases to 25% if the condition changes to $\omega' < 10f$.

Higher percentages follow if a linear mean flow is added, as in figure 5.2, or if the initial intrinsic frequency is reduced; however, as long as $c/U_0 \lesssim 1$ at the initial position, the merging of rays continues to be split between shears of positive and negative sign.

At higher phase speeds (figure 5.5), the number of convergences is reduced. Again, convergence is not limited to regions of positive shear nor to waves of low frequency. The final value of $\omega'$ falls below its initial value of $10f$ in less than half of the cases plotted in figure 5.5. We also note that since a high intrinsic frequency corresponds to a low ratio of $m/k$, focussing affects more than just the shortest vertical wavelengths. If focussing develops when $\omega' = 10f$, for instance, it takes a horizontal wavelength of only 500 meters to give a vertical wavelength of 100 meters.

The value of $\partial m/\partial z$ is one of several initial conditions left unchanged so far. It has been set to zero, indicating that there is no initial convergence to a bundle of rays. To test whether the results depend as critically on this parameter as they do in the case of steady shears, where the value of $\partial m/\partial z$ accounts for the difference between the Hartman and BB solutions (Chapter 2), the following example is considered.

Suppose high frequency waves can propagate a vertical distance of one or two inertial wavelengths before the current changes markedly. If the waves are generated, for example, by shear instability, then $\omega$ is constant and $\partial m/\partial z$ can be derived from the dispersion relation. For short times,

$$\frac{\partial m}{\partial z} = \frac{\partial m}{\partial \omega'} \frac{\partial \omega'}{\partial z}$$

$$= \frac{k^2 \omega'}{(\omega'^2 - f^2)^{3/2}} \frac{N^2 - f^2}{(N^2 - \omega'^2)^{1/2}} \frac{\partial U}{\partial z} \operatorname{sgn} m \, . \qquad (5.21)$$

This is used as an initial condition; for longer times, $\omega$ is allowed to vary and the system evolves according to (5.6)-(5.9).

Figure 5.6 contrasts this initial state (figure 5.6a) with one in which $\omega'$ is independent of depth (figure 5.6b). The integrations begin at $t = \frac{1}{4}T_i$ with $\omega/N = .2$ and $c/U_0 = 1.4$ in the former case and $\omega'/N = .2$ and $c'/U_0 = 1.4$ in the latter case. The rays originating from $.4 < z < .75$ in figure 5.6a illustrate that divergence in one region may strengthen convergence in another. Whether the amplitudes increase in a bundle of rays is thus as much a question of where the rays end up relative to the phase of the inertial oscillation as the degree of convergence with which they start.

Integrations based on (5.21) and run at 12 starting times covering an inertial period show patterns similar to those plotted in figure 5.5. In part this is because the differences between the constant-$\omega$ and constant-$\omega'$ initial conditions decrease as the magnitude of the inertial current decreases; however, even when the current is strong, the difference in the location of instabilities relative to the phase of the current tends to lessen as the calculations proceed beyond an inertial period.

The sensitivity of the ray solutions to changes in $k/\beta$ is shown in figure 5.7, which contains the ray trajectories for the interval between $t = 0$ and the time indicated in the plots. The value of $k/\beta$ labels each curve. The trajectories for $k/\beta = .40$ in figures 5.7a,b correspond to those in figure 5.1a and in figure 1.1 (with $z = .3\lambda_i$ at $t = 0$) respectively. The former is an example in which convergence is not associated with critical layers, while the latter models the critical-layer interaction as closely as any of the results shown thus far.

The final spread of trajectories in figure 5.7a is less than half a vertical wavelength of the short waves (approximately $.2\lambda_i$ at $t = 1.4T_i$), but the solutions are more sensitive to variations in $k/\beta$ than is revealed by the trajectories. For $k/\beta = .44, .40$ convergence develops at $t = 1.4T_i$, while for $k/\beta = .38, .36$ $E$ normalized by its initial value remains small for over 2½ inertial periods. This dramatic change in the intrinsic energy density for slight changes in the independent parameter is a characteristic feature of the ray solutions.

In figure 5.7b, convergence occurs in all three cases at approximately the same depth and time ($t = .1T_i$) despite a spread of ±25% in horizontal wavenumber. This suggests that convergence in this example is not limited to narrow-banded wave packets. The effects of bandwidth are considered in the next section.

### C. Dispersion and geometrical spreading

Dispersion results from the dependence of $\mathbf{C}_g$ on the magnitude of $\mathbf{K}$, while geometrical spreading results from the dependence of $\mathbf{C}_g$ on the direction of $\mathbf{K}$. These processes are analyzed in this section using ray theory to determine their effects of the convergence of localized, short-wave packets.

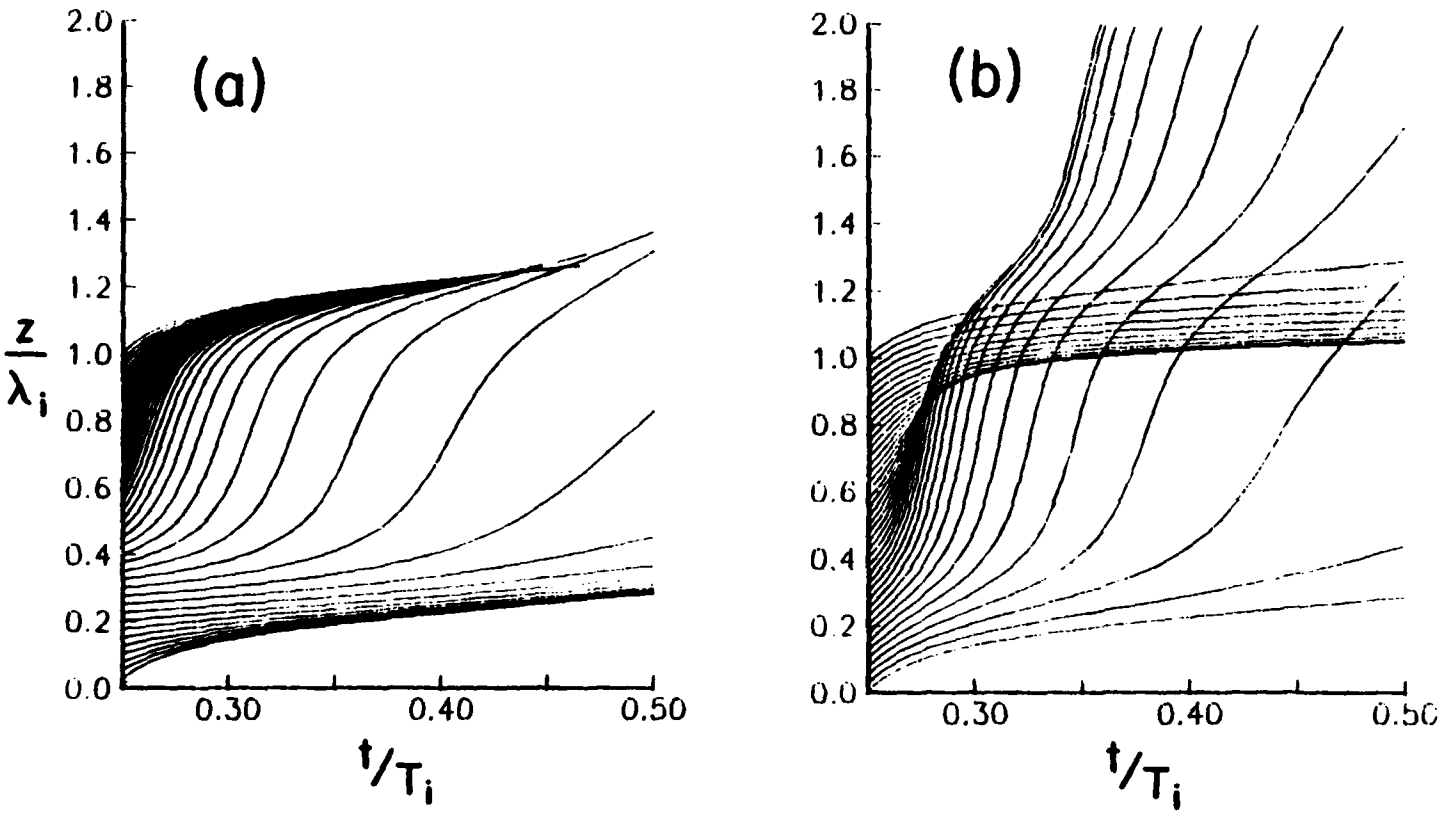


**Figure 5.6.** Ray paths for two initial values of $\partial m/\partial z$. In both cases, the initial time is $\frac{1}{4}T_i$. In (*a*), $\partial m/\partial z$ takes the value obtained in (5.15), corresponding to $\omega$ independent of depth, while in (*b*), $\partial m/\partial z=0$, corresponding to $\omega'$ independent of depth.

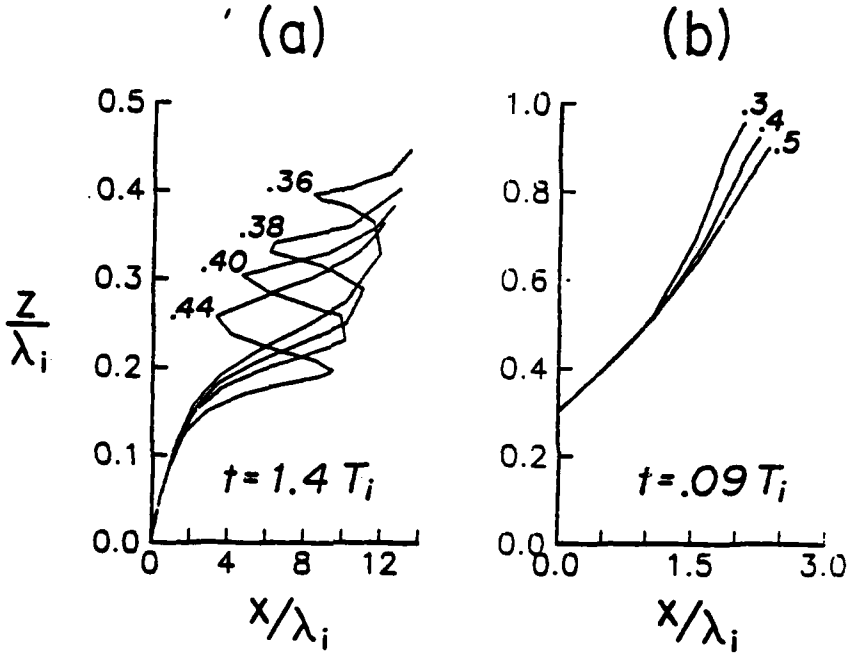


Figure 5.7. Ray paths for different values of $k/\beta$. The value of $k/\beta$ marks each ray path.

The importance of dispersion and geometrical spreading depends on the wavenumber bandwidth of the packet. Bandwidth has been ignored thus far, under the premise (verified below) that the results capture the essential features of at least narrow-banded wave packets. With bandwidth neglected, changes in the action density $A$ have been attributed entirely to refraction, as though all the energy resides in a single value of $\mathbf{K}$ and $\omega$ at each depth and time. A finite bandwidth is implied, however, since the action propagates at the group velocity, not the phase velocity.

Ray theory can be used to study the processes of dispersion and geometrical spreading. Suppose, for example, that a source localized in space and time generates a broad-banded wavefield, as in the "seas" of surface waves. As the Fourier components spread due to their difference in group velocities, as in the "swell" region, a gradient in $\mathbf{K}$ develops. Strictly speaking, all wavenumbers are present everywhere, but to a first approximation, one wavenumber is dominant at each position with all others destructively interfering. This gives rise to a nonzero $\nabla\mathbf{K}$ even if the medium is uniform, which when substituted into the ray equation for the action density $A$ describes the changes in packet shape resulting from dispersion and geometrical spreading. Thus bandwidth information enters through the value of $\nabla\mathbf{K}$.

This discussion is exactly the physical justification for the method of stationary phase, and, in fact, ray theory can be used to derive the stationary-phase result

$$A \sim t^{-n} \ , \tag{5.22}$$

for large $t$, where n is the number of spatial dimensions. To demonstrate this, we consider the simple case of one-dimensional propagation in a uniform medium. (The generalization to $n$ dimensions is given in Appendix B.) Since the wavenumber $k$ is then conserved,

$$k = k(x - C_g t) \ , \tag{5.23}$$

where $C_g$ is the group velocity. Implicit differentiation with respect to $x$ leaves

$$\frac{\partial k}{\partial x} = \left(\frac{\partial k}{\partial x}\right)_0 \left\{1 - t\ \Omega_{kk}\ \frac{\partial k}{\partial x}\right\}$$

$$= \left(\frac{\partial k}{\partial x}\right)_0 \left\{1 + t\ \Omega_{kk} \left(\frac{\partial k}{\partial x}\right)_0\right\}^{-1} \ . \tag{5.24}$$

where $(\partial k/\partial x)_0$ is the value of $\partial k/\partial x$ at $t = 0$. Substituting (5.24) into the one-dimensional action equation

$$\frac{dA}{dt} = -\ A\ \Omega_{kk}\ \frac{\partial k}{\partial x} \tag{5.25a}$$

(see (5.8)) gives in the long-time limit

$$\frac{dA}{dt} = -\frac{A}{t}\,, \tag{5.25b}$$

and leads to the asymptotic behavior given by (5.22) provided $\Omega_{kk}\,\partial k/\partial x > 0$ at $t = 0$.

The advantage that ray theory has over the method of stationary phase is that it is easily extended to nonuniform media. Complications arise because in general $\partial k/\partial x$ is not known analytically and because in three dimensions, (5.24), or (5.10), must be replaced by the system of equations

$$\frac{d\nabla\mathbf{K}}{dt} = -\nabla\mathbf{K}\;\Omega_{\mathbf{KK}}\;\nabla\mathbf{K} - \nabla\mathbf{K}\;\Omega_{\mathbf{x}\mathbf{K}} - \Omega_{\mathbf{K}\mathbf{x}}\;\nabla\mathbf{K} - \Omega_{\mathbf{x}\mathbf{x}}\,, \tag{5.26}$$

(Hayes, 1970). (Only six of the equations in (5.26) are independent since the tensor $\nabla\mathbf{K}$ is symmetric.) The components of $\Omega_{\mathbf{KK}}$, which are listed at the end of Appendix B, include $\Omega_{kk}$, $\Omega_{kl}$, $\Omega_{km}$ and so forth, and similarly for $\Omega_{\mathbf{x}\mathbf{K}}$ and $\Omega_{\mathbf{x}\mathbf{x}}$.

We use (5.26), the action equation in three dimensions

$$\frac{dA}{dt} = -A\;\nabla\mathbf{K} : \Omega_{\mathbf{KK}}\,, \tag{5.27}$$

and the ray equations (5.5)-(5.7) to include the effects of dispersion and geometrical spreading with those of refraction.

The results are presented in figure 5.8, which shows the intrinsic energy density $E$ normalized by its initial value as a function of time for several ray calculations. The number that labels each curve, which for later reference we call $\gamma$, has the same magnitude as *each* of the terms

$$\frac{1}{m^2}\,\frac{\partial m}{\partial z}\,,\ \frac{1}{k^2}\left\{\frac{\partial k}{\partial x}\,,\ \frac{\partial k}{\partial y}\,,\ \frac{\partial k}{\partial z}\,,\ \frac{\partial l}{\partial y}\,,\ \frac{\partial l}{\partial z}\right\} \tag{5.28}$$

and has positive (negative) sign when the rays are initially divergent (convergent). For initial divergence (convergence), the sign of each component of $\nabla\mathbf{K}$ is chosen to have the same (opposite) sign as the corresponding component of $\Omega_{\mathbf{KK}}$, so that all nine terms contributing to the dyadic product in (5.27) have the same sign. This maximizes the effects of dispersion and geometrical spreading.

In figure 5.8a, the initial conditions are those used in figure 5.1 except for the value of $\gamma$. (The bold curve corresponds to the calculation in figure 5.1.) For $\gamma > 0$, dispersion and geometrical spreading are important for times less than about half an inertial period. Refractive

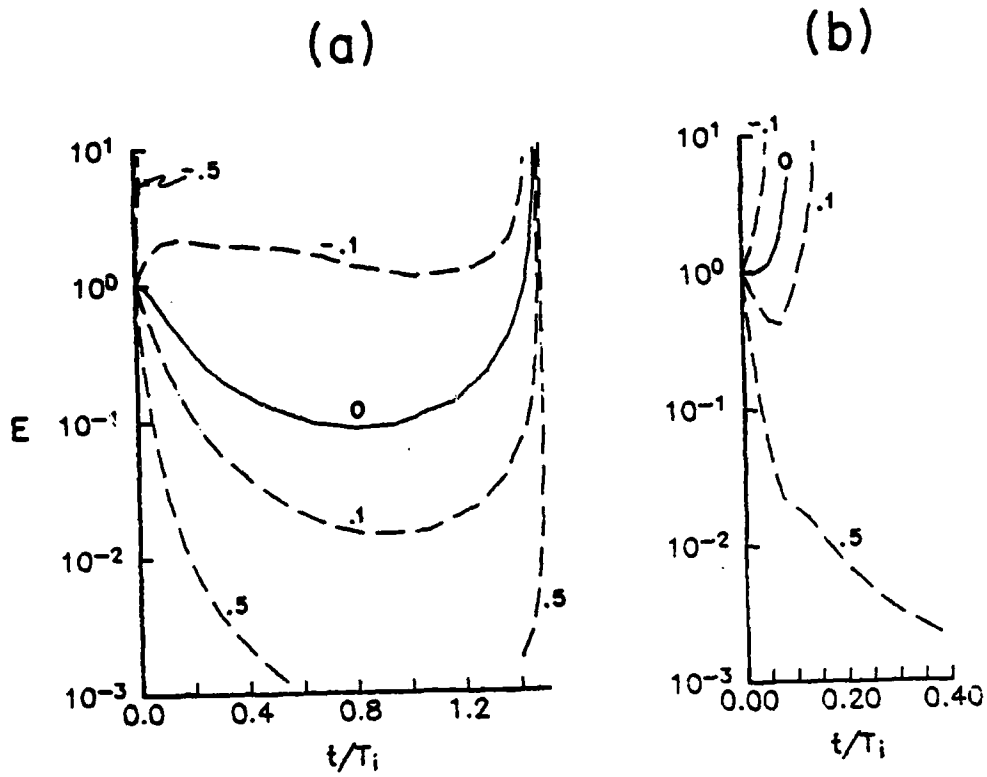


Figure 5.8. The effects of dispersion and geometrical spreading. Each curve is labeled by the value of $\gamma$. The magnitude of $\gamma$ is the magnitude of each of the terms in (5.28), while the sign of $\gamma$ is positive for initially divergent rays and negative for initially convergent rays.

The ray path and the values of $\omega'$, $c$, $C_{g3}$, and $m$ for (*a*) are shown in figure 5.1. For (*b*), the ray path is the one originating at $z = .3\lambda_i$ in figure 1.1.

convergence becomes the dominant process after $1.2T_i$, and the results illustrate the explosive growth in E that this convergence produces. As in nearly all the ray solutions summarized in this chapter, there is no question as to when focussing occurs.

In the case where $\gamma = -.5$ in figure 5.8a, the rays are so sharply focussed at the outset that unstable amplitudes are shortly reached. In the Taylor-Goldstein model, this degree of convergence is produced by a current with low Richardson number (see (3.9)). In the present context, the focussing arises because the initial conditions place Fourier components with slow group velocities ahead of those with fast group velocities. The ray equations then predict convergence without background currents.

The second example (figure 5.8b) shows the effects of dispersion and geometrical spreading in a situation resembling the critical-layer interaction. Here the initial conditions (except for the values of $\gamma$) are the same as for the ray that begins at $z = .3\lambda_i$ in figure 1.1. The wave group thus encounters a decelerating current with positive shear, as in the experiments of Thorpe (1981). In the case with no initial convergence (the bold curve in figure 5.8b), unstable amplitudes are reached after only one-tenth of an inertial period.

For $\gamma = \pm.1$ this result does not change appreciably, so the case of small bandwidth is similar to the case of zero bandwidth. This agrees with the conclusions of BB, who claim (page 535) that "...a wave packet clustered around a single wave-number $k_0$ does not behave qualitatively differently from a single wave-number...", and the result is expected from the laboratory study of Thorpe (1981). In Thorpe's experiments, a rough estimate of the bandwidth in horizontal wavenumbers $\delta k/k$ is $1/n_x$ where $n_x$ is the number of horizontal wavelengths to the corrugated lower boundary of Thorpe's tank. Thorpe uses the two values $n_x = 8$ and $n_x = 16$. In addition, there is the bandwidth in frequency associated with the time dependent current in Thorpe's study.

For the larger value of $\gamma = .5$, the spreading of Fourier components dominates the convergence due to refraction by the currents. This example resembles the Hartman result more than the critical-layer interaction (for the times shown in the figure) because the energy is not being concentrated at one depth. The intrinsic energy density remains small relative to its initial value until $t = T_i$, when convergence occurs.

As mentioned above, the basis for using ray theory in these examples is the assumption that the wavefield can be described locally by one value of K and $\omega$ at each time; however, measurements suggest that the deep-ocean internal wave field more closely resembles the "seas" of surface waves more than the "swell" since many wavenumbers and frequencies exist at each position. We must therefore deal with rays that start at the same location with different wavenumbers, as pictured in the plots of figure 5.7, and with rays that arrive at the same

position and time through different trajectories.

The quantitative analysis of a short-wave spectrum in inertial shears will not be considered here, except to mention that in treating a spectrum, it is convenient to introduce a spectral density for action, which we denote by $n(\mathbf{K},\mathbf{x},t)$ to distinguish it from $A(\mathbf{x},t)$, the action density of a single wavetrain in physical space. The equation governing conservation of $n$ is (Holloway 1981)

$$n_t + \Omega_{k_j} n_{x_j} - \Omega_{x_j} n_{k_j} = 0 \tag{5.29}$$

which reduces to (5.8) when

$$n(\mathbf{K},\mathbf{x},t) = A(\mathbf{x},t)\delta(\mathbf{K}-\mathbf{K}(\mathbf{x},t)) \tag{5.30}$$

(J. Lerner, unpublished manuscript). The subscript $j$ in (5.29) indicates a summation over the components of $\mathbf{K}$ and $\mathbf{x}$.

By regarding the phases of the short waves as random, the action and energy densities in physical space may be written as

$$\int n(\mathbf{K},\mathbf{x},t)\,d\mathbf{K} \tag{5.31}$$

$$\int n(\mathbf{k},\mathbf{x},t)\,\Omega'(\mathbf{k},\mathbf{x},t)\,d\mathbf{K} \tag{5.32}$$

respectively, where $\Omega'$ is the intrinsic frequency. It is the value of the integrals in (5.31) and (5.32) and not the spectral densities by themselves that should determine whether unstable amplitudes are reached. The evaluation of these integrals would seem to be a necessary step toward understanding the mechanisms by which internal waves dissipate.

# CHAPTER 6

## CONCLUSION

When the background current is an inertial oscillation, the process by which short waves are focussed to high amplitudes differs in significant ways from the steady-shear case. As the ray tracing calculations of Chapter 5 emphasize, a critical-layer interaction offers only one example of convergence, one in which refraction leads to a decrease in the intrinsic frequency toward $f$ and the group velocity toward zero. In inertial shears, other possibilities are equally likely. The intrinsic frequency may be high or increasing, so that wave groups are accelerating when convergence develops. Inertial shears also can leave the rays sharply focussed at depths where $\partial U/\partial z$ vanishes and at times when $U$ is identically zero. The magnitude and sign of the shear, therefore, provide little indication of the likeliness for short-wave convergence when $c \lesssim U_0$ (figure 5.4).

The results also differ from those of steady-shear analyses in that the condition $c \leqslant U_0$ does not guarantee that the waves will shortly attain high amplitudes or develop unstable shears. This is due to the reversing nature of the inertial currents, both in space and time, which can delay or prevent convergence and allow the short waves to persist for several inertial periods without becoming unstable (figure 5.2). By contrast, instabilities arise within a few Vaisala periods in the studies of Fritts (1978), Hartman (1975), and Thorpe (1981). Fritts (1982) points out this difference between steady and time dependent currents.

The reversing currents also negate Hartman's mechanism of dissipation (shear instability without an accompanying increase in $E$). However, short waves may induce instability without reaching large amplitudes if they propagate into an inertial current that is by itself marginally stable.

The conditions that give rise to critical-layer interactions match those studied by Thorpe (1981): a decelerating current coupled with a mean shear of the sign necessary to decrease the intrinsic frequency of the short waves in the direction of propagation. This combination of deceleration and refraction leads to a rapid growth of the short-wave amplitudes. Here again, though, differences appear in relation to steady shears, since wave groups with phase speeds exceeding the mean-flow maximum by two or three times, and the local mean-flow velocity by much more, are focussed to unstable amplitudes by the inertial currents.

These results indicate the difficulty in defining a critical-layer interaction quantitatively. The criterion $c = U$, which suffices in the Taylor-Goldstein model, is artificial in the present context, because waves of higher phase speeds are similarly amplified by the currents. There is

no obvious limit to the values of $c$ or the intrinsic frequency $\omega'$ at the time of focussing that can be used to distinguish the critical-layer interaction from other convergences. One possibility is to associate with critical layers all convergences with a decreasing $\omega'$ along the ray (i.e. all those falling in the hatched sections of figures 5.4 and 5.5), but this would include behavior much different from the results of BB for the reasons mentioned above and in Chapter 5. To avoid the difficulties in definition, and to designate all focussings induced by currents whether associated with critical layers or not, we use the term *refractive convergence.*

The qualitative features of refractive convergence are shown schematically in figure 6.1. The arrows represent a pair of adjacent group velocity vectors, whose orientations change through refraction by an inertial current. This example corresponds to the situation in figure 5.1, although the range of angles of the vectors relative to the vertical and relative to each other is exaggerated for illustration purposes.

The vectors, which begin parallel, remain so in the second diagram of figure 6.1 ($t = T_i/8$). The action density stays approximately constant during this time interval (cf. figure 5.1f), so the dynamics are similar to those predicted by Hartman (1975), not by the Taylor-Goldstein model. Divergence begins thereafter and continues when the current vanishes at $t=T_i$ (again unlike the Taylor-Goldstein model). Convergence takes over after $t = \frac{1}{4}T_i$, intensifying in the last diagram of the sequence at a level where the shear is negative.

Once underway, refractive convergence typically leads to sudden increases in $E$ —— so sudden, in fact, that a clear distinction exists between those waves that reach high amplitudes and those that do not. Because there are few intermediate cases, the findings are not sensitive to the criterion for identifying a convergence event (page 25).

The calculations of Chapter 5 are based on ray theory. Chapters 3 and 4 are devoted to assessing the errors in this approach. A comparison with solutions to the Taylor-Goldstein equation finds partial reflection to be unimportant for waves with a Doppler-shifted phase speed barely exceeding the mean flow maximum; however, WKB techniques perform poorly when the curvature term $U_{zz}/(c-U)$ dominates the others in the coefficient of the Taylor-Goldstein equation. The solutions then resemble shear modes (solutions to the Rayleigh equation) rather than internal wave modes, and the internal wave dispersion relation is of little use, even qualitatively. The example shown in figure (4.1) illustrates that a turning point can appear at a depth where the ray equations predict a small and decreasing intrinsic frequency.

Chapter 4 finishes with a discussion of the inappropriateness of the Taylor-Goldstein model for short waves in a inertial current. The reasons include the time dependence of the shear and the nonzero vertical gradient in the Doppler-shifted frequency $\omega$ that a time-dependent shear induces.

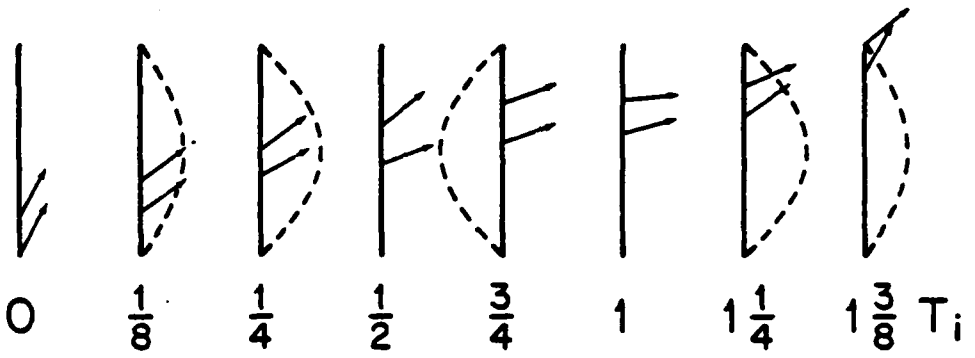


Figure 6.1. The process of refractive convergence. The illustration shows schematically the changing orientation of a pair of adjacent group velocity vectors. The conditions correspond to those depicted in figure 5.1. The lengths, angles, and vertical separation of the vectors are not properly scaled. The horizontal separation need not be considered, since the wave amplitudes and inertial current do not depend on horizontal position. The profiles of $U$ are indicated by dashed lines, and the time in inertial periods is given below each diagram.

The vectors begin parallel, diverge for times between $T_i/8$ and $3T_i/4$, and converge for later times. Convergence strengthens in the final diagram at a depth where the shear is negative.

Near convergence zones, the equations fail because of the small-amplitude approximation. Numerical solutions to the nonlinear equations and laboratory experiments show overturning in the vicinity of the critical layer, but in a "noisy" ocean wave-wave interactions may limit wave growth before the critical layer is reached. The conditions for triad instability, for instance, may be realized before those for gravitational or shear instability. Holloway (1981, 1982) addresses these points and cautions against ignoring the nonlinear interactions of a random wave field in critical-layer studies.

There are also linear processes to be examined that may affect the focussing of short-wave energy. For example, it should be useful to analyze with the ray calculations a broad banded, short-wave spectrum propagating through random, low-frequency shears.

The results presented here cover a very limited range of the numerous independent variables, which include $J$, $\beta$, $N/f$, and the initial values of $\omega'$, $m$, and $\partial m/\partial z$. Although critical-layer interactions similar to those studied by Thorpe (1981) can be identified in inertial currents, these results show that convergence may develop in ways that do not resemble critical-layer interactions at all. The calculations reveal the importance of the more general process of *refractive convergence*, which operates under a broad range of conditions. Because of its connection with dissipation, refractive convergence merits attention for the same reasons previously attached to critical layers by BB, Thorpe (1981), Hartman (1975), Fritts (1978, 1982), Munk (1980) and others: to improve our understanding on the subjects of short-wave dynamics, the internal-wave energy budget, and mixing processes in the deep-ocean.

## References


Andrews, D.G. & M.E. McIntyre 1978 On wave-action and its relatives. *J. Fluid Mech.* **89**, 647-664.

Booker, J.R. & F.P. Bretherton 1967 The critical layer for internal gravity waves in a shear flow. *J. Fluid Mech.* **27**, 513-539.

Bretherton, F.P. 1966 The propagation of groups of internal gravity waves in a shear flow. *Quart. J. Roy. Meteor. Soc.* **92**, 466-480.

Brown, S.N. & K. Stewartson 1980 On the algebraic decay of disturbances in a stratified fluid. *J. Fluid Mech.* **100**, 811-816.

Bulirsch, R. & J. Stoer 1966 Numerical treatment of ordinary differential equations by extrapolation methods. *Numerische Math.* **8**, 1-13.

Drazin, P.G. 1958 The stability of a shear layer in an unbounded heterogeneous inviscid fluid. *J. Fluid Mech.* **4**, 214-224.

Epstein, P.S. 1930 Reflection of waves in an inhomogeneous absorbing media. *Proc. Nat. Acad. Sci.* **16**, 627-637.

Fritts, D.C. 1978 The nonlinear gravity wave-critical layer interaction. *J. Atmos. Sci.* **35**, 397-413.

Fritts, D.C. 1982 The transient critical-level interaction in a Boussinesq fluid. *J. Geophys. Res.* **87**, 7997-8016.

Garrett, C.J.R. 1968 On the interaction between internal gravity waves and a shear flow. *J. Fluid Mech.* **34**, 711-720.

Goldstein, S. 1931 On the stability of superposed streams of fluids of different densities. *Proc. Roy. Soc. Lond.* **A132**, 524-548.

Hartman, R.J. 1975 Wave propagation in a stratified shear flow. *J. Fluid Mech.* **71**, 89-104.

Hayes, W.D. 1970 Kinematic wave theory. *Proc. Roy. Soc. Lond. A* **320**, 209-226.

Holloway, G. 1980 Oceanic internal waves are not weak waves. *J. Phys. Oceanog.* **10**, 906-914.

Holloway, G. 1981 Theoretical approaches to interactions among internal waves. In *Nonlinear*

*Properties of Internal Waves*, A.I.P. Conference Proceedings No. 76, American Institute of Physics, New York, 37-67.

Jones, W.L. 1967 Propagation of internal gravity waves in fluids with shear and rotation. *J. Fluid Mech.* **30**, 439-448.

Jones, W.L. 1968 Reflexion and stability of waves in stably stratified fluids with shear: a numerical study. *J. Fluid Mech.* **34**, 609-624.

Koop, C.G. 1981 A preliminary investigation of the interaction of internal gravity waves with a steady shearing motion. *J. Fluid Mech.* **113**, 347-386.

LeBlond, P.H. & L.A. Mysak 1978 *Waves in the Ocean.* Elsevier Scientific Publishing Co., New York.

Meyer, R.E. 1980 Exponential asymptotics. *SIAM Rev.* **22**, 213-223.

Mied, R.P. & J.P. Dugan 1975 Internal wave reflection by a velocity shear and density anomaly. *J. Phys. Oceanog.* **5**, 279-287.

Miles, J.W. 1961 On the stability of heterogeneous shear flows. *J. Fluid Mech.* **10**, 496-508.

Miles, J.W. 1963 On the stability of heterogeneous shear flows. Part 2. *J. Fluid Mech.* **16**, 209-227.

Munk, W.H. 1981 Internal waves and small-scale processes. In *Evolution of Physical Oceanography*, B.A. Warren and C. Wunsch eds., MIT Press, 264-291.

Mysak, L.A. 1976 A kinetic theory for internal waves in a randomly stratified fluid. *Dyn. Atmos. Oceans* **1** 91-98.

Olver, F.W.J. 1974 *Asymptotics and Special Functions.* Academic Press, New York.

Phillips, O.M. 1966 *The Dynamics of the Upper Ocean.* Cambridge University Press, London and New York.

Pinkel, R. 1981 On the use of Doppler sonar for internal wave measurements. *Deep-Sea Res.* **28**, 269-289.

Sanford, T.B. 1975 Observations of the vertical structure of internal waves. *J. Geophys. Res.* **80**, 3861-3871.

Snow, C.S. 1942 The Hypergeometric and Legendre Functions with Applications to Integral

Equations of Potential Theory. National Bureau of Standards.

Thorpe, S.A. 1969 Neutral eigensolutions of the stability equation for stratified shear flow. *J. Fluid Mech.* **36**, 673-683.

Thorpe, S.A. 1978 On internal gravity waves in an accelerating shear flow. *J. Fluid Mech.* **88**, 623-639.

Thorpe, S.A. 1981 An experimental study of critical layers. *J. Fluid Mech.* **103**, 321-344.

van Duin, C.A. & H. Kelder 1982 Reflection properties of internal gravity waves incident upon a hyperbolic tangent shear layer. *J. Fluid Mech.* **120**, 505-521.

## APPENDIX A.

## THE REFLECTED AND TRANSMITTED WAVE AMPLITUDES IN TERMS OF HEUN FUNCTIONS.

In chapter four, it is shown that the the solution corresponding to the reflected wave as $z \to -\infty$ is expressed in terms of the Heun's function as

$$w_1 = F(c_1,b;\bar{\alpha},\bar{\beta},\gamma,\delta;U_1) \ . \tag{A1}$$

This is the solution in (4.14) about $U_1 = 0$ with zero-exponent. The solution with exponent $-2i\mu_1$ corresponds to the incident wave as $z \to -\infty$ and can be written in terms of Heun's function using the transformation $w_2 = U_1^{-2i\mu_1} w_1$. From Snow (1942),

$$w_2 = U_1^{2i\mu_1} F(c_1,b_2;1+\alpha-\gamma,1+\beta-\gamma,\delta;U_1) \ , \tag{A2a}$$

where

$$b_2 = b - (1-\gamma)\{\delta+c_1(1+\bar{\alpha}+\bar{\beta}-\gamma-\delta)\} \ . \tag{A2b}$$

The solution belonging to the zero-exponent at $U_1 = 1$ in (4.14) corresponds to the transmitted wave as $z \to +\infty$. Transforming $U_1 \to 1-U_1$ leads to the solution (Snow, page 123)

$$w_3 = F(1-c_1,-b-\bar{\alpha}\bar{\beta};\bar{\alpha},\bar{\beta},1+\bar{\alpha}+\bar{\beta}-\gamma-\delta,\delta;1-U_1) \ . \tag{A3}$$

To obtain the amplitudes of the reflected and transmitted waves, the solutions $w_1$ and $w_2$ must be related to the solution $w_3$. For the Hypergeometric functions, these connection formulae can be expressed in terms of gamma-functions, but for Heun's functions, it is necessary to match the solutions and their derivatives at points between the singularities. The matching point must be positioned at a distance less than $(c_1-1)$ away from $U_1 = 1$ to be within the radius of convergence of $w_3$. If we denote this position by $x$, it follows that

$$R = -\left[\frac{w'_2 w_3 + w_2 w'_3}{w'_1 w_3 + w_1 w'_3}\right]_x \tag{A4}$$

and

$$T = \left[\frac{w_2 w'_1 - w'_2 w_1}{w_3 w'_1 + w'_3 w_1}\right]_x \tag{A5}$$

where a prime indicates differentiation with respect to $U_1$ and the subscript $x$ implies that all functions are evaluated at $U_1 = x$.

The numerator in (A5) is the negative of the Wronskian for the two solutions $w_1$ and $w_2$, which we evaluate as

$$w_1 w'_2 - w'_1 w_2 = (w_1 w'_2 - w'_1 w_2)_{U_1=0} e^{-\int_0^{U_1} p dz} \tag{A6}$$

where $p$ is the coefficient of $w_{U_1}$ term in Heun's equation (4.8). Substituting for $p$ leaves

$$T = -\left( \frac{1-\gamma}{U_1^{\gamma}(1-U_1)^{1+\alpha+\beta-\gamma-\delta}(1-\frac{U_1}{c_1})^{\delta}} \cdot \frac{1}{w_3 w'_1 + w'_3 w_1} \right)_x . \tag{A7}$$

The same procedure can be applied to the case involving a critical layer within the shear region, although a branch cut must be chosen. A lengthy calculation, which will not be given here, leads to the results presented in figure A1 and in Munk (1980) for $c=0$. (Van Duin & Kelder (1982) give a simpler technique for determining the reflection and transmission coefficients.) Waves are overreflected when $|R|^2 \geqslant 1$, which requires $Ri < .13$.

For values in the unstable region of the $\alpha - J$ plot of figure A1 (Drazin, 1958), an infinite, reflected, intrinsic energy density is obtained. This is the case of resonant overreflection. According to linear theory, the shear layer radiates waves without being forced.

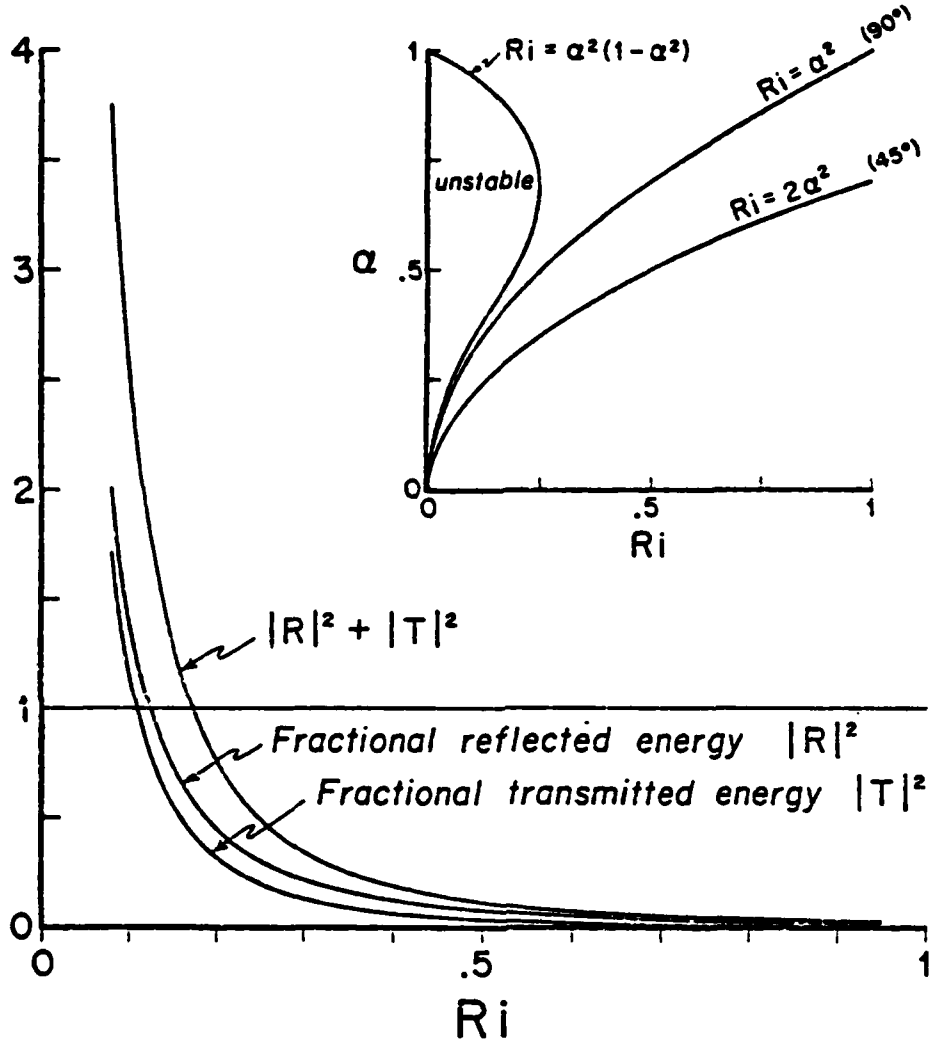


Figure A1. Reflection from a critical layer. Plotted are the values of the fractional intrinsic energy density reflected and transmitted through a mean shear flow, $U=U_0 \tanh\beta z$ as a function of minimum Richardson number $J=N^2/(\beta^2 U_0^2)$. The plot is drawn for $J=2\alpha^2$, where $\alpha=k\beta$ is the dimensionless horizontal wavenumber. This corresponds to a wave packet traveling at an inclination of 45° as $z\to\pm\infty$. ($Ri=\alpha^2$ corresponds to the limiting case of vertical group velocity as $z\to\pm\infty$.)

## APPENDIX B.

## CHANGES IN PACKET AMPLITUDE DUE TO DISPERSION AND GEOMETRICAL SPREADING.

Using ray theory, we derive equations that describe the dispersion and geometrical spreading of a localized wave packet in a uniform medium of $n$ dimensions. The derivation generalizes the one presented in Section C of Chapter 5 and leads to the stationary-phase result

$$A \sim t^{-n} \tag{B1}$$

for large times.

In a uniform medium, the ray equation for the action density $A$ takes the form

$$\frac{dA}{dt} = -A \frac{\partial^2 \Omega}{\partial k_i \partial k_j} \frac{\partial k_j}{\partial x_i} \tag{B2}$$

(Hayes, 1970), where the subscripted variables are components of $\mathbf{K}$ and $\mathbf{x}$, repeated indices are summed over all values, and the dispersion relation is

$$\omega = \Omega(\mathbf{K}(\mathbf{x},t)) \quad . \tag{B3}$$

(For convenience in notation we do not use subscripts for partial derivatives in this appendix.)

To obtain $\partial k_i/\partial x_j$, we write

$$\mathbf{K} = \mathbf{K}(\mathbf{x} - \mathbf{C}_g t) \quad , \tag{B4}$$

appropriate to a uniform medium, and define

$$\alpha = \mathbf{x} - \mathbf{C}_g t \tag{B5}$$

Differentiating (B4) with respect to $\mathbf{x}$ leaves

$$\begin{aligned} \frac{\partial k_i}{\partial x_j} &= \frac{\partial k_i}{\partial \alpha_p} \frac{\partial \alpha_p}{\partial x_j} \\ &= \frac{\partial k_i}{\partial \alpha_p} \left\{ \delta_{pj} - t \frac{\partial}{\partial x_j} C_{gp} \right\} \\ &= \frac{\partial k_i}{\partial \alpha j} - t \left\{ \frac{\partial k_i}{\partial \alpha_p} \frac{\partial^2 \Omega}{\partial k_p \partial k_m} \frac{\partial k_m}{\partial x_j} \right\} \quad . \end{aligned} \tag{B6}$$

where $\partial k_k/\partial \alpha_j$ is the value of $\partial k_i/\partial x_j$ at $t = 0$. We rewrite (B6) as

$$\frac{\partial k_m}{\partial x_j}\left\{\delta_{mi} + t\,\frac{\partial k_i}{\partial \alpha_p}\,\frac{\partial^2 \Omega}{\partial k_p\,\partial k_m}\right\} = \frac{\partial k_i}{\partial \alpha_j}\ , \tag{B7}$$

which in the long-time limit becomes

$$\frac{\partial k_m}{\partial x_j}\left\{\frac{\partial k_i}{\partial \alpha_p}\,\frac{\partial^2 \Omega}{\partial k_p\,\partial k_m}\right\} = \frac{1}{t}\,\frac{\partial k_i}{\partial \alpha_j}\ . \tag{B8}$$

Multiplying (B8) by $\partial \alpha_q / \partial k_i$ and using

$$\frac{\partial \alpha_q}{\partial k_i}\,\frac{\partial k_i}{\partial \alpha_p} = \delta_{pq} \tag{B9}$$

leaves

$$\frac{\partial k_m}{\partial x_j}\,\frac{\partial^2 \Omega}{\partial k_p \partial k_m}\,\delta_{pq} = \frac{1}{t}\,\delta_{qj}\ . \tag{B10}$$

We use the relation $\delta_{jj} = n$, where $n$ is the number of spatial dimensions, and set $q = j$ in (B10) to obtain

$$\frac{\partial k_m}{\partial x_j}\,\frac{\partial^2 \Omega}{\partial k_j \partial k_m} = \frac{n}{t} \tag{B11}$$

substituting (B11) into the action equation (B2) gives

$$\frac{dA}{dt} = -A\,\frac{n}{t} \tag{B12}$$

or

$$At^n = constant\ , \tag{B13}$$

which matches the stationary-phase result (B1).

We note the following:

(i) Equation (B7) applies to those components of **K** that lie in a direction in which the medium is homogeneous, even if the medium is not homogeneous in all directions.

(ii) Not all initial conditions lead to the result given by (B13). If, in (B7),

$$\frac{\partial^2 \Omega}{\partial k_p\,\partial k_m}\,\frac{\partial k_i}{\partial \alpha_p} < 0\ , \tag{B14}$$

then the term in parentheses in (B7) can become zero, giving an infinite value for $\partial k_m / \partial x_j$ and for the action density. Physically, the Fourier components with slow group

velocities precede those with faster group velocities at the initial time, and as the fast waves overtake the slow ones, a caustic develops.

(iii) We list here for use in Section C of Chapter 5 the components of $\partial^2\Omega/(\partial k_i\,\partial k_j)$. The dispersion relation is

$$\Omega(k) = \left\{\frac{(k_1^2 + k_2^2)N^2 + m^2f^2}{k_1^2 + k_2^2 + m^2}\right\}^{1/2} \tag{B15}$$

$$= \left(\frac{a}{b}\right)^{1/2} \tag{B16}$$

where $\mathbf{K} = (k_1, k_2, m)$ and

$$a \equiv (k_1^2 + k_2^2)N^2 + m^2f^2 \tag{B17}$$

$$b \equiv (k_1^2 + k_2^2 + m^2) \ . \tag{B18}$$

Then for $i = 1, 2$,

$$\frac{\partial^2\Omega}{\partial k_i^2} = m^2(N^2 - f^2)(a^{-1/2}b^{-3/2})\left\{1 - k_i^2(3b_{-1} + N^2a^{-1})\right\} \tag{B19}$$

$$\frac{\partial^2\Omega}{\partial k_1\partial k_2} = -m^2(N^2 - f^2)(ab)^{-3/2}\,k_1k_2(3a + bN^2) \tag{B20}$$

$$\frac{\partial^2\Omega}{\partial k_i\partial m} = mk_i(N^2 - f^2)(a^{-1/2}b^{-3/2})\left\{2 - m^2(3b^{-1} + f^2a^{-1})\right\} \ , \tag{B21}$$

with $\partial^2\Omega/\partial m^2$ given by (5.10).

## APPENDIX C

## WAKES AND MEAN FLOWS OF LOW-FREQUENCY INTERNAL-WAVE PACKETS*

### A. Introduction

The role of wave transience in affecting mean flows and mean profiles of temperature and tracers is well-established, a prime example being the sudden stratospheric warming, where growing planetary waves modify the temperature distribution by as much as 40°C and decelerate upper level winds.

Transience is a marked feature of energetic, near-inertial oscillations in the ocean. Although it is unlikely that they will cause ocean temperatures to increase by 40°C, these oscillations could be very effective at inducing mean flows. If, as for high-frequency, plane internal wave packets,

$$\bar{u} \sim \bar{u}^L \sim O(\frac{E}{c'}) , \tag{C1}$$

where $\bar{u}$ and $\bar{u}^L$ are the Eulerian and Lagrangian horizontal mean velocities, respectively, $E$ is the intrinsic energy density (see equation (C16) and below), and $c'$ is the horizontal, intrinsic phase velocity, then for fixed horizontal wavelength, the generation of mean velocities would be heavily dominated by low-frequency waves: in addition to the phase velocity appearing in the denominator in (C1), energy spectra typically fall off as the inverse square of the frequency and even faster near the inertial and tidal bands. A rough calculation using (C1) and the observation that low-frequency waves are marginally stable (i.e. have a minimum Richardson number approaching unity), gives mean-flow magnitudes of nearly half the orbital velocity of the waves.

When Coriolis terms are important, however, mean flows can evolve differently. Here mean-flow equations are derived for low-frequency internal wave packets. Of the cases considered, only when rotation is ignored does $\bar{u}$ or $\bar{u}^L$ equal E/c identically, and only when horizontal dependence is ignored does an inertial wave appear in the wake of the packet, as predicted by Hasselmann (1970) for a wave field that is statistically homogeneous in the horizontal. These calculations supplement the related work of Andrews (1980), Bretherton (1969), Grimshaw (1975), and Hasselmann (1970).

*References are included at the end of this Appendix.

It is assumed that the Vaisala frequency $N$ is constant and that there is no background current. For the upper thermocline, where low-frequency packets are most energetic and identifiable, these are poor assumptions, but they help to isolate the dependence of mean-flow evolution on wave frequency. The calculations can probably be extended to include variations in the medium through a WKB analysis without altering the conclusions obtained below. We also ignore ocean boundaries, which is reasonable for the scales to be considered: vertical packet dimensions of a few hundred meters, implying horizontal wavelengths of roughly 5-20 kilometers, depending on frequency.

The equations to be solved are

$$\mathbf{u}_t + \mathbf{u}\cdot\nabla\mathbf{u} + 2\boldsymbol{\Omega}x\mathbf{u} + \frac{1}{\rho_0}\nabla p + \mathbf{g} = 0 \tag{C2a}$$

$$\nabla\cdot\mathbf{u} = 0\,. \tag{C2b}$$

The fluid is nondissipative, Boussinesq, and incompressible, $2\boldsymbol{\Omega} = (0,0,f)$, where $f$ is the inertial frequency, assumed constant, and $\mathbf{u} = (u,v,w)$.

**B. Mean flows**

As waves propagate through a fluid, they induce stresses that can accelerate mean motions. There are many examples with physical interpretations in the literature. Mathematically, a mean flow arises because a sinusoid is generally not an exact solution to the equations of motion. If sinusoidal motion is assumed, the nonlinear terms generate harmonics and mean quantities. Even in the special cases where sinusoidal motion is an exact solution (e.g. plane internal-inertial gravity waves in a uniform, nondissipative, Boussinesq fluid) strictly sinusoidal motion may not be consistent with the condition of no motion initially. For instance, a wave packet with a slowly growing leading edge induces mean as well as orbital motion. Where the amplitude of the wave packet is constant, the horizontal velocity is $u = \epsilon\sin(\mathbf{K}\cdot\mathbf{x}-\omega t) + \bar{u}$, where $\bar{u}$ is an $O(\epsilon^2)$ constant. This is still an exact solution under the assumptions mentioned above provided that $\omega$ is the Doppler-shifted frequency, related to the intrinsic frequency $\omega'$ by $\omega = \omega' + Uk$ for $k>0$.

When rotation (and dissipation) can be ignored, net accelerations produced by the leading edge of a wave packet are cancelled by decelerations in the trailing edge. The mean flow returns to zero after the packet passes, although a net displacement of the fluid occurs if the Lagrangian-mean flow is nonzero.

When rotation is important, the trailing edge may not decelerate the fluid back to zero velocity because the mean motion, now affected by the Coriolis force, changes direction during the passage of the packet. The same forces that set up the motion, therefore, may no longer stop it. Instead, the system is left ringing at inertial frequency after the packet propagates away. This is illustrated in the following example.

Solutions to (C2) are sought of the form

$$(u,v,w,p,\theta) = (u',v',w',p',\theta') + (\bar{u},\bar{v},\bar{w},\bar{p},\bar{\theta}) \ . \tag{C3}$$

The buoyancy parameter is $\theta = g\rho'/\rho_0$ and a factor of $1/\rho_0$ is included in the pressure variable for simplicity in notation. The primed quantities are $O(\epsilon)$ and behave like $\sin(\mathbf{K}\cdot\mathbf{x} - \omega t)$, where $\mathbf{K} = (k,0,m)$. The barred quantities are obtained by an Eulerian average over phase and are $O(\epsilon^2)$.

The $O(\epsilon)$ equations,

$$u'_t - fv' + p'_x = 0 \tag{C4}$$

$$v'_t + fu' + p'_y = 0 \tag{C5}$$

$$w'_t + \theta' + p'_z = 0 \tag{C6}$$

$$\theta'_t - N^2 w' = 0 \tag{C7}$$

$$u'_x + v'_y + w'_z = 0 \ , \tag{C8}$$

yield the linear-theory results: the dispersion relationship

$$\omega'^2 = \frac{k^2N^2+m^2f^2}{k^2+m^2} \tag{C9}$$

and the relationships

$$(u',w',p',\theta') = \left(\frac{i\omega'}{f} \ , -i\frac{\omega' k}{fm} \ , \frac{i(N^2-\omega'^2)k}{fm^2} \ , -\frac{N^2 k}{fm}\right) v' \tag{C10}$$

(Andrews, 1980).

The $O(\epsilon^2)$ equations describe the evolution of means and second harmonics. The later component is eliminated by averaging, leaving

$$\mu\bar{u}_T - f\bar{v} + \mu\bar{p}_X = -\mu(\overline{u'^2})_X - \mu(\overline{u'w'})_Z \tag{C11}$$

$$\mu\bar{v}_T + f\bar{u} + \mu\bar{p}_Y = -\mu(\overline{v'^2})_Y \tag{C12}$$

$$\mu\bar{w}_T + \bar{\theta} + \mu\bar{p}_Z = -\mu(\overline{u'w'})_X - \mu(\overline{w'^2})_Z \tag{C13}$$

$$\mu\bar{\theta}_T - N^2\bar{w} = -\mu(\overline{v'\theta'})_Y \tag{C14}$$

$$\mu(\bar{u}_X + \bar{v}_Y + \bar{w}_Z) = 0\,. \tag{C15}$$

These equations are written in terms of the stretched variables $X = \mu x$, $T = \mu t$ ($\mu << 1$) which vary by an $O(1)$ amount over the scales of the packet. The boundary condition specifies that all quantities vanish as $Z \to -\infty$ (envisioning a packet with downward group velocity). The $O(\epsilon)$ equations have been used to eliminate products of quantities on the right-hand-side of (C11)-(C15) which are out of phase. The mass source in the Lagrangian-mean continuity equation (C15) does not appear for this problem until $O(\epsilon^4)$.

Case (1) $\partial/\partial X = \partial/\partial Y = 0$, $f\tau_p \sim O(1)$

By ignoring variations in $X$ and $Y$, the continuity equation and boundary condition force $\bar{w}$ to be zero everywhere. The buoyancy equation then gives $\bar{\theta} = 0$, leaving the pressure gradient term to balance the Reynolds stresses in the vertical momentum equation.

A high frequency approximation, $\omega'/f >> 1$, reduces the equation for the $x$-component of the pseudomomentum, $\hat{p}_1$, to

$$\hat{p}_{1T} = -(\overline{u'^2})_X - (\overline{u'w'})_Z \tag{C16}$$

where to $O(\epsilon^2)$, $\hat{p}_1 = E/c'$ and $E = (\overline{u'^2} + \overline{v'^2} + \overline{w'^2} + \overline{\theta'^2}/N^2)/2$, and $c' = \omega'/k$. The horizontal momentum equations then become

$$\mu\bar{u}_T - f\bar{v} = \mu\hat{p}_{1T} \tag{C17}$$

$$\mu\bar{v}_T + f\bar{u} = 0\,. \tag{C18}$$

At this stage we assume that the Coriolis terms and the acceleration terms are the same order, i.e. that $f\tau_p \sim O(1)$, where $\tau_p$ is the time scale of the packet. (Since $\tau_p >> 1/\omega'$ is necessary for scale separation, this assumption includes the high frequency approximation leading to (C16)). The case of strong rotation, $f\tau_p >> 1$ is considered in the next section.

Defining $\bar{\phi} = \bar{u} + i\bar{v}$, (C17) and (C18) combine to become

$$\mu\bar{\phi}_T - if\bar{\phi} = \mu\hat{p}_{1T}\,, \tag{C19}$$

which has the solution

$$\bar{\phi} = \frac{E}{c} - ife^{i(f/\mu)T}\int_{-\infty}^{T} e^{-i(f/\mu)T'}\frac{E}{c}(T')\,dT'\,. \tag{C20}$$

The second term arises when $f$ is nonzero and represents an inertial wave left in the wake of the packet. Hasselmann (1970) obtains a similar solution for a random field of surface waves or internal waves in shallow water. Related behavior illustrating that Rossby-wave packets leave lower-frequency Rossby waves in their wake is shown in Rhines and Holland (1979).

It therefore appears that transient waves need not induce transient mean flows, even in a nondissipative fluid. This conclusion follows more directly when the equations are rewritten in Lagrangian-mean form:

$$\mu\bar{u}^L_t - f\bar{v}^L + \bar{p}^L_x = -\mu(\overline{p\xi_x})_X - \mu(\overline{p\zeta_x})_Y - \mu(\overline{p\eta_x})_Z$$

$$= \mu\hat{p}_{1T} \tag{C21}$$

$$\mu\bar{v}^L_t + f\bar{u}^L + \bar{p}^L{}_Y = 0 \tag{C22}$$

$$\mu\bar{w}^L_t + \bar{\theta}^L + \bar{p}^L{}_Z - \mu(\overline{p\xi_z})_X - \mu(\overline{p\zeta_z})_Y - \mu(\overline{p\eta_z})_Z$$

$$= -\mu\hat{p}_{3T} \tag{C23}$$

$$\mu\bar{\theta}^L_t - N^2\bar{w}^L = 0 \tag{C24}$$

$$\mu(\bar{u}^L_X + \bar{v}^L_Y + \bar{w}^L_Z) = 0 \tag{C25}$$

where $\xi(x,t) = (\xi,\zeta,\eta)$ is the particle displacement, and the psuedomomemtum vector $\hat{\mathbf{p}}$ has components $(\hat{p}_1,0,\hat{p}_3)$. The Lagrangian mean, defined as

$$\overline{g(x,t)}^L = \overline{g(x+\xi,t)} \tag{C26}$$

for any quantity $g$, is an ensemble average over phase. It is then possible to define $\xi$ such that $\overline{\xi(x,t)} = 0$ identically (Andrews & McIntyre (1978)). Dependence on $X$ and $Y$ in (C21)-(C25) has been included for later reference. Ignoring these dependences for now, the $X$-momentum equation can be rewritten as

$$\mu(\bar{u}^L - \hat{p}_1)_T - f\bar{v}^L = 0\,, \tag{C27}$$

which in turn can be rewritten as

$$\bar{D}^L(\bar{u}^L - \hat{p}_1 - fy) = 0$$

(Andrews & McIntyre (1978)). $\bar{D}^L$ signifies the rate of change moving with the Lagrangian-mean flow:

$$\bar{D}^L = \frac{\partial}{\partial T} + \bar{u}^L \cdot \frac{\partial}{\partial X} . \tag{C28}$$

If the Coriolis force leads to a net change in $y$ during the passage of the packet, $\bar{u}^L$ must remain nonzero after the packet propagates away.

**Case (2)** $\partial/\partial X = \partial/\partial Y = 0$ $f\tau_p >> 1$

The solution given in (C20) is derived assuming that the Coriolis terms are small but nonzero. This requires

$$\frac{f\bar{v}^L}{\mu\partial\bar{u}^L/\partial T} = \frac{f^2\bar{v}^L}{P}\mu^2\partial^2\bar{v}^L/\partial T^2 \sim f^2\frac{T^2}{\mu^2} \sim O(1) . \tag{C29}$$

We identify $\tau_p \equiv T/\mu$ with the time scale of the packet. Let $\tau_p = 2\pi n/\omega'$ with $n$ measuring the number of wave periods required for the wave packet to reach maximum amplitude at a fixed location. Then $f\tau_p \sim O(1)$ translates to $\omega' \sim O(2\pi nf)$. If $n = 4$, say, $\omega'$ must be in the range of $25f$ for the Coriolis and acceleration terms to be of the same order. Since $25f$ corresponds to a wave period of less than one hour at midlatitudes, this division lies above the frequency of the semidiurnal tide and tidal harmonic at six-hour period. The assumption $f\tau_p \sim O(1)$ therefore excludes what is by far the most energetic part of the oceanic internal wave spectrum. The amount that is excluded depends of course on $n$, but the point is that it is $2\pi nf/\omega'$ and not $f/\omega'$ that measures the ratio of the Coriolis to acceleration terms in the mean equations.

The approximate balance to lowest order is now between the Coriolis terms and the radiation stresses, so that

$$\bar{v}^L = -\frac{\mu}{f}\hat{p}_{1T} \tag{C30}$$

$$\bar{u}^L = \frac{\mu^2}{f^2}\hat{p}_{1TT} . \tag{C31}$$

Because the mean motion is reduced to an $O(\mu)$ quantity, the Stokes drift appears at the same order

$$\bar{v}^S = (\overline{\eta' v'})_Z . \tag{C32}$$

More interestingly, $\bar{v}^L$ and $\bar{u}^L$ return to zero after the packet propagates away. If the mean velocities are expanded in powers of $\mu$, inertial motion in the wake still does not appear, for at all higher orders $\bar{v}^L$ and $\bar{u}^L$ can be related to higher-order derivatives of $\hat{p}_1$ with respect to $T$.

To see what has happened to the inertial motion, we can derive an exact solution for $\bar{\phi}^L = \bar{u}^L + i\bar{v}^L$ analogous to (20) for $\bar{\phi}$ except that when written in terms of Lagrangian-mean variables, the solution is valid for all frequencies: no high-frequency approximation is necessary to replace the right hand sides of (C21) and (C23) with $\hat{p}_{1T}$ and $\hat{p}_{3T}$ respectively. (Pseudomomentum is not exactly conserved for localized wave packets since mean quantities depend on position; however, corrections do not appear in the present context until $O(\epsilon^4)$.) We can thus write

$$\bar{\phi}^L = \int_{-\infty}^{T} e^{i(f/\mu)(T-T')}\mu\hat{p}_{1T'}dT' . \tag{C33}$$

Since by assumption $f\tau_p >> 1$, the phase of the exponential function in the integrand of (C33) varies rapidly. An asymptotic expansion can then be found through an integration by parts. Integrating $N$ times leaves

$$\bar{\phi}^L = -i\frac{\mu}{f}\hat{p}_{1T} + \cdots + i^N\mu^N\int_{-\infty}^{T} e^{i(f/\mu)(T-T')}\frac{\partial^N\hat{p}_1}{\partial T'^N}dT' . \tag{C34}$$

The last integral represents the inertial motion left in the wake of the packet. It does not appear in the asymptotic expansion because it is exponentially small as $\mu \to 0$. (Using a stationary-phase calculation and noticing that the phase function in the integral has no stationary points, the integral can be shown to be exponentially small as $\mu$ vanishes (Lighthill, 1978).)

**Case (3)** $\partial/\partial X, \partial/\partial Y \sim O(1)$; $f\tau_p >> 1$

Low-frequency, internal wave packets have horizontal scales that are much greater than their vertical scales; however, unlike Hasselmann (1970), we consider horizontal variations because the ratio of the Reynolds stress terms in the x-momentum equation, for example, is

$$\frac{(\overline{u'^2})_X}{(\overline{u'w'})_Z} \sim \frac{m}{k}\frac{\Delta Z}{\Delta X}, \tag{C35}$$

where $\Delta Z$ and $\Delta X$ are the vertical and horizontal scales of the packet. The ratio thus scales as the number of horizontal wavelengths to the number of vertical wavelengths, not as the ratio of absolute packet dimensions or wavenumbers. A similar argument applies to the radiation stresses in the Lagrangian-mean equations.

Allowing for the packet to produce mean horizontal pressure gradients and allowing for all the terms in the continuity equation leaves the system of equations given in (C21)-(C25).

We write

$$\bar{v}^L = v^{(0)} + \mu v^{(1)} + \mu^2 v^{(2)} + \cdots , \tag{C36}$$

and similarly for all other mean quantities, and attempt an expansion which balances terms geostrophically and hydrostatically at lowest order:

$$-fv^{(0)} + p_X^{(0)} = 0 \tag{C37}$$

$$fu^{(0)} + p_Y^{(0)} = 0 \tag{C38}$$

$$\theta^{(0)} + p_Z^{(0)} = 0 \tag{C39}$$

$$u_X^{(0)} + v_Y^{(0)} = 0 . \tag{C40}$$

A stream function, $\psi^{(0)}$, can be defined at this order, related to $p^{(0)}$ by

$$f\nabla_h^2\psi^{(0)} = \nabla_h^2 p^{(0)} , \tag{C41}$$

where $\nabla_h^2 = \partial^2/\partial X^2 + \partial^2/\partial Y^2$, $u^{(0)} = -\psi_Y^{(0)}$, and $v^{(0)} = \psi_X^{(0)}$.

The evolution of the $O(1)$ quantities is obtained from the $O(\mu)$ equations:

$$u_T^{(0)} - fv^{(1)} + p_X^{(1)} = \hat{p}_{1T} \tag{C42}$$

$$v_T^{(0)} + fu^{(1)} + p_Y^{(1)} = 0 \tag{C43}$$

$$w_T^{(0)} + \theta^{(1)} + p_Z^{(1)} = \hat{p}_{3T} \tag{C44}$$

$$\theta_T^{(0)} - N^2 w^{(1)} = 0 \tag{C45}$$

$$u_X^{(1)} + v_Y^{(1)} + w_Z^{(1)} = 0 \tag{C46}$$

These can be manipulated, using (C41), to obtain Poisson's equation for $\psi^{(0)}$

$$\nabla_h^2\psi^{(0)} + \frac{f^2}{N^2}\psi_{ZZ}^{(0)} = -\hat{p}_{1Y} . \tag{C47}$$

The formal solution to (C47) can be written in terms of a Green's function or derived using a three-dimensional Fourier transform.

Suppose we choose a Gaussian packet envelope:

$$\hat{p}_1 \sim \exp\{-\alpha_1^2(X - C_{g1}T)^2 - \alpha_2^2 Y^2 - \alpha_3^2(Z - C_{g3}T)^2\} \tag{C48}$$

where $\mathbf{C}_g = (C_{g1}, 0, C_{g3})$ is the group velocity. Symmetry considerations lead to

$$(\psi_X^{(0)} = p_X^{(0)} = \psi_Z^{(0)} = p_Z^{(0)})_{Y=0} = 0 \,, \tag{C49}$$

so $\bar{v}^L$ is zero along the $Y$-centerline of the packet, where the wave amplitude reaches a maximum.

In the far-field, $\psi^{(o)}$ and $p^{(o)}$ decay as $1/r^2$ multiplied by some angular dependence. (An electromagnetic analogy is the potential due to a dipole source.) Consequently, no inertial wake results. Viewed another way, (47) becomes Laplace's equation as $T \to \infty$, X fixed, which, because of the boundary conditions, cannot support motion.

As in Case (2) the inertial motion does not appear at higher order. The $O(\mu^2)$ equations give

$$\nabla_h^2 p^{(1)} + \frac{f^2}{N^2} p_{ZZ}^{(1)} = \hat{p}_{1XT} + \frac{f^2}{N^2} \hat{p}_{3ZT} \,, \tag{C50}$$

which also reduces to Laplace's equation after the packet propagates away. Similarly, the $O(\mu^3)$ equations lead to

$$\nabla_h^2 p^{(2)} + \frac{f^2}{N^2} p_{ZZ}^{(2)} = -w_{ZT}^{(1)} \left( 1 + \frac{f^2}{N^2} \right) . \tag{C51}$$

Since the structure of the equation at all higher orders is the same as (C51), the expansion yields only decaying motion in the packet wake.

Again as in Case (2), the inertial motion may result from an expression which is exponentially small as $\mu \to 0$. There is at least one other possibility though: the inertial wake may be limited to packets of infinite horizontal extent, i.e. the limit of $\partial/\partial X$, $\partial/\partial Y$ approaching zero may be a singular one. The idea is that although the horizontal pressure gradients build slowly in a long but finite packet, they can eventually reach an $O(1)$ magnitude. The dynamics change when horizontal pressure gradients are important and inertial oscillations may disappear.

An exact solution to (C21)-(C25) would reveal whether the limit $\partial/\partial X$, $\partial/\partial Y \to 0$ is singular. A suggestion made by Glenn Flierl (personal communication) is to try a one-cycle sinusoidal packet

$$\hat{p}_1 \sim \sin\lambda \,, \quad \lambda = (\boldsymbol{\alpha} \cdot \mathbf{X} - \alpha T) \,, \tag{C52}$$

for $-\pi \leq \lambda \leq \pi$ and $\hat{p}_1 = 0$ otherwise. This allows solutions to be obtained by assuming behavior of the form $A\cos\lambda + B\sin\lambda$ for each of the mean variables. To meet the initial

condition, solutions to the homogeneous equations are also needed. The effect of discontinuities in $\hat{p}_{1TT}$ at $\lambda = -\pi,\pi$ requires assessment.

Another possibility is to ignore $Z$ dependence. The equations then reduce to

$$\mu\bar{u}^L_T - f\bar{v}^L + \mu\bar{p}^L_X = \mu\hat{p}_{1T} \tag{C53}$$

$$\mu\bar{v}^L_T + f\bar{u}^L + \mu\bar{p}^L_Y = 0 \tag{C54}$$

$$\mu(\bar{u}^L_X + \bar{v}^L_Y) = 0\,, \tag{C55}$$

which can be combined to give the "wake-less" equation

$$\nabla^2\psi = \hat{p}_{1Y}\,; \tag{C56}$$

however, if $X$ and $Y$ variations are ignored from the outset, so the forcing, $\hat{p}_{1T}$, builds in time everywhere by the same amount, then the governing equation becomes the "wake-full" equation (C19). This model, although somewhat contrived, is an example illustrating the singular limit associated with the neglect of horizontal dependences.

### C. Nonuniform media and changes in packet amplitude

Grimshaw (1975) derives a general system of mean flow equations that allows for variations in the Vaisala frequency and for background shears. Even in a uniform medium, however, the wave induced mean flow will be affected by changes in packet amplitude resulting from dispersion and geometrical spreading, especially when the propagation is three-dimensional and especially when the waves are highly transient or localized and therefore involve a broad (or at least non-narrow) range of frequencies and wavenumbers. A stationary-phase calculation describes the attenuation of energy in a uniform medium, but this result can also be obtained from the ray equations. The equation for action density along the ray (in one dimension for now) is

$$\frac{dA}{dt} = -A\{\Omega_{kx} + \Omega_{kk}\frac{\partial k}{\partial x}\}\,, \tag{C57}$$

where $\omega(x,t) = \Omega(k,x,t)$ is the dispersion relation and $d/dt = \partial/\partial t + C_g\,\partial/\partial X$. Since $dk/dt = 0$

$$k_x = \{k(x-C_g t)\}_x = \frac{(k_x)_{t=0}}{1+\Omega_{kk}(k_x)_{t=0}t}\,. \tag{C58}$$

Substituting (C58) into (C57) and using $\Omega_{kx} = 0$, gives the stationary phase result that the action density decays as $1/t$ as $t \to \infty$.

It may seem surprising that although dispersion results from a spread in frequencies or wavenumbers, bandwidth information does not enter directly into the equation for action density, as it does in the equation for action spectral density $n(k,x,t)$:

$$\frac{\partial n}{\partial t} + \frac{\partial n}{\partial k}\frac{dk}{dt} + \frac{\partial n}{\partial x}\frac{dx}{dt} = 0 . \tag{C59}$$

Here spectral content appears through the term $\partial n/\partial k$; recall, however, that the bandwidth does not enter in the stationary phase calculation either, except at higher order when developed as an asymptotic expansion (Felsen and Marcuvitz, 1973). Writing

$$\xi(x,t) = \int_{-\infty}^{\infty} g(k) e^{i\psi(k)t} dk , \tag{C60}$$

where $\psi(k) = kx/t - \omega(k)$, we transform variables, using

$$s^2 = i(\psi(k_c) - \psi(k)) \tag{C61}$$

$$G(s) = g(k)\frac{dk}{ds} = g(k)\frac{2is}{\psi'(k)} . \tag{C62}$$

(Note that using L'Hopital's rule,

$$G(0) = g(k_0)\sqrt{\frac{2i}{\psi''(k_0)}} \tag{C63}$$

provided $\psi''(k_0)$ is nonzero.) Equation (C60) then becomes

$$\xi = e^{i\psi(k_0)} \int_{-\infty}^{\infty} (G(0) + G'(0)s + G''(0)\frac{s^2}{2} + \cdots) e^{-s^2 t} ds . \tag{C64}$$

The stationary point is $k_0$, which satisfies $\psi'(k_0) = 0$, and a prime in (C63) denotes differentiation with respect to $s$. The bandwidth information in $G'(0)$, $G''(0)$ $\cdots$ appears only as a correction to the lowest-order solution.

The advantage of the ray equation (C57) over the method of stationary phase is that it is easily extended to nonuniform media. Complications arise because in general $k_x$ is not known analytically and because in three dimensions, nine equations (six of which are independent) are required:

$$\frac{d}{dt}\nabla\mathbf{K} = -\nabla\mathbf{K}\cdot\Omega_{\mathbf{KK}}\cdot\nabla\mathbf{K} - \Omega_{\mathbf{xK}}\cdot\nabla\mathbf{K} - \nabla\mathbf{K}\cdot\Omega_{\mathbf{Kx}} - \Omega_{\mathbf{xx}} \tag{C65}$$

(Hayes, 1970). Still the system of equations can be integrated numerically. As an approximation, it is probably justified to ignore horizontal variations in the Vaisala frequency and shear, so that the horizontal wavenumbers are conserved, but the point here is that for localized packets, dispersion and geometrical spreading due to a spread in horizontal wavenumbers should not be dismissed as unimportant. Its affect on packet amplitudes may match that produced by refraction.

**Conclusion**

The character of the mean flow induced by an internal wave packet is sensitive to the frequency of the waves and the dimensions of the packet.

When horizontal variations are neglected, high-frequency waves induce a mean flow given by $\bar{u}^L = E/c$, unless rotation is included. Then $\bar{u}^L$ is given by (C20) and an inertial wave oscillates in the wake of the packet. As the wave frequency decreases toward f, the mean flow adjusts so as to move perpendicular to **K** at lowest order; moreover, in contrast to the high-frequency case, $\bar{u}^L$ vanishes whenever the packet amplitude levels off (see (C29) and (C30)).

When horizontal dependences are included, the lowest order, mean flow equations lead to Poisson's equation for the pressure or stream function regardless of wave frequency. Motions induced by low frequency packets balance hydrostatically and geostrophically. A question suggested by these calculations is whether the limit $\partial/\partial X, \partial/\partial Y \rightarrow 0$ is a singular one, and thus whether it is realistic to expect wakes with inertial oscillations.

Table 1 provides a summary of results.

**Acknowledgements**

The work presented in this appendix was done while the author participated in the Summer Program in Geophysical Fluid Dynamics at the Woods Hole Oceanographic Institution. Thanks are due to Professors Glenn Flierl, Joe Keller and Russ Davis for valuable discussions.

REFERENCES

Andrews, D.G. 1980 On the mean motion induced by transient inertio-gravity waves. *Pageoph 118*, 177-188.

Andrews, D.G. and M.E. McIntyre 1978 An exact theory of nonlinear waves on a Lagrangian-mean flow. *J. Fluid Mech. 89*, 609-646.

Bretherton, F.P. 1969 On the mean motion induced by internal gravity waves. *J. Fluid Mech. 37*, 785-803.

Felsen, L.B. & N. Marcuvitz 1973 *Radiation and Scattering of Waves.* Prentice-Hall, Inc., New Jersey. 888 pp.

Grimshaw, R. 1975 Nonlinear internal waves in a rotating fluid. *J. Fluid Mech. 71*, 497-512.

Hasselmann, K. 1970 Wave-driven inertial oscillations. *Geophys. Fluid Dyn. 1*, 463-502.

Hayes, W.D. 1970 Kinematic wave theory. *Proc. Roy. Soc. Lond. A 320*, 209-226.

Lighthill, J. 1978 *Waves in Fluids.* Cambridge University Press, London. 504 pp.

Rhines, P.B. and W.R. Holland 1979 A theoretical discussion of eddy-driven mean flows. *Dyn. Atm. Oceans 3*, 289-325.

| $\frac{\partial}{\partial X} = \frac{\partial}{\partial Y} = 0$ | Mean Flow Equation | Accuracy | Inertial Wake |
|---|---|---|---|
| $f = 0$ | $\bar{u}^L = E/c\,;\ \bar{v}^L = 0$ | Exact to $O(\varepsilon^2)$ | No |
| $f\tau_p \sim O(1)$ | $\bar{\phi}^L = E/c - if\int_{-\infty}^{T} e^{i(f/\mu)(T-T')}\,\frac{E(T')}{c}\,dT'$ | " | Yes |
| $f\tau_p \gg 1$ | $\bar{v}^L = -\frac{\mu}{f}\hat{p}_{1T}\,;\ \bar{u}^L = \frac{\mu^2}{f^2}\,\hat{p}_{1T}$ | $O(\mu^2\varepsilon^2)$ | Exponentially small as $\mu \to 0$ |
| $\frac{\partial}{\partial X} = \frac{\partial}{\partial Y} \sim O(1)$ | | | |
| $f = 0$ | $\nabla_h^2\psi^{(0)} = -\hat{p}_{1Y}$ | $O(\mu\varepsilon^2)$ | No |
| $f\tau_p \sim O(1)$ | " | " | Exponentially small or absent |
| $f\tau_p \gg 1$* | $\nabla_h^2\psi^{(0)} + \frac{f^2}{N^2}\,\psi_{ZZ}^{(0)} = -p_{1Y}^{*}$ | " | Exponentially small or absent |

*Geostrophic and hydrostatic at $O(\mu^0\varepsilon^2)$.

Table C1. Properties of wave-induced mean flows.

9/82

# MANDATORY DISTRIBUTION LIST

## FOR UNCLASSIFIED TECHNICAL REPORTS, REPRINTS & FINAL REPORTS

## PUBLISHED BY OCEANOGRAPHIC CONTRACTORS

## OF THE OCEAN SCIENCE AND TECHNOLOGY DIVISION

## OF THE OFFICE OF NAVAL RESEARCH

Department of Defense

Office of the Secretary of Defense (3)
Assistant Director of Defense Research & Engineering
Washington, D.C. 20301

Navy

Office of Naval Research (3)
Code 460
Arlington, VA 22217

Office of Naval Research
Code 480
Arlington, VA 22217

Office of Naval Research
Code 102 B
Arlington, VA 22217

Office of Naval Research
Commanding Officer
1030 East Green Street
Pasadena, CA 91101

Naval Ocean Research & Development Activity
NORDA, Code 300
NSTL Station
Bay St. Louis, MS 39529

Naval Research Laboratory (6)
Library, Code 2620
Washington, D.C. 20375

U.S. Naval Oceanographic Office
Library, Code 8170
NSTL Station
Bay St. Louis, MS 39529

Other Government Agencies

Defense Documentation Center (12)
Cameron Station
Alexandria, VA 22314

National Oceanic & Atmospheric Administration
National Oceanographic Data Center
Washington Navy Yard
Rockville, MD 20852